Am J Cancer Res 2026;16(1):314-337
www.ajcr.us /ISSN:2156-6976/ajcr0170038

Original Article

Increasing autophagy activity suppresses *Helicobacter pylori* infection-related gastric cancer tumorigenesis both *in vitro* and *in vivo*

Pei-Wen Lin[1], Yu-Wen Liu[1], Man-Ling Chu[1], Yu-Cing Chen[1], Yao-Hsiang Shih[2], Yu-Chun Ma[3], Pin-Yuan Lin[4], I-Ying Kuo[5], Hong-Yi Chang[2], Li-Tzong Chen[6], Jaw-Yuan Wang[6,7,8,9,10], Ying-Ray Lee[1,11,12,13,14], Chao-Hung Kuo[15,16,17,18], Deng-Chyang Wu[15,16,17], Hsiao-Sheng Liu[1,6,19]

[1]Tropical Medicine, Kaohsiung Medical University, Kaohsiung 807378, Taiwan; [2]Department of Anatomy, School of Medicine, College of Medicine, Kaohsiung Medical University, Kaohsiung 807378, Taiwan; [3]Department of Pathology, Kaohsiung Medical University Hospital, Kaohsiung Medial University, Kaohsiung 807378, Taiwan; [4]Life Sciences, College of Life Science, Kaohsiung Medical University, Kaohsiung 80708, Taiwan; [5]Department of Biotechnology, College of Life Science, Kaohsiung Medical University, Kaohsiung 80708, Taiwan; [6]Center for Cancer Research, Kaohsiung Medical University, Kaohsiung 807378, Taiwan; [7]Division of Colorectal Surgery, Department of Surgery, Kaohsiung Medical University Hospital, Kaohsiung Medical University, Kaohsiung 807378, Taiwan; [8]Department of Surgery, Faculty of Medicine, College of Medicine, Kaohsiung Medical University, Kaohsiung 807378, Taiwan; [9]Graduate Institute of Clinical Medicine, College of Medicine, Kaohsiung Medical University, Kaohsiung 807378, Taiwan; [10]Graduate Institute of Medicine, College of Medicine, Kaohsiung Medical University, Kaohsiung 807378, Taiwan; [11]Department of Microbiology and Immunology, College of Medicine, Kaohsiung Medical University, Kaohsiung 807378, Taiwan; [12]Faculty of Post-Baccalaureate Medicine, College of Medicine, Kaohsiung Medical University, Kaohsiung 807378, Taiwan; [13]Center for Tropical Medicine and Infectious Disease, Kaohsiung Medical University, Kaohsiung 807378, Taiwan; [14]Department of Medical Research, Kaohsiung Medical University Hospital, Kaohsiung 807378, Taiwan; [15]Division of Gastroenterology, Department of Internal Medicine, Kaohsiung Medical University Hospital, Kaohsiung 807378, Taiwan; [16]Regenerative Medicine and Cell Therapy Research Center, Kaohsiung Medical University, Kaohsiung 80756, Taiwan; [17]Department of Medicine, Faculty of Medicine, College of Medicine, Kaohsiung Medical University, Kaohsiung 807378, Taiwan; [18]Division of Gastroenterology, Department of Internal Medicine, Kaohsiung Show Chwan Memorial Hospital, Kaohsiung 821011, Taiwan; [19]Medical Research Center, Kaohsiung Medical University Hospital, Kaohsiung Medical University, Kaohsiung 807378, Taiwan

Received November 16, 2025; Accepted January 11, 2026; Epub January 15, 2026; Published January 30, 2026

Abstract: *Helicobacter pylori* (*H. pylori*) infection is a major risk factor for gastric cancer (GC). Although autophagy is involved in *H. pylori* infection, its role in *H. pylori*-associated tumorigenesis remains unclear. Here, we investigated whether enhancing autophagy suppresses GC malignancy under *H. pylori* infection. Autophagy and mitochondrial markers were analyzed in GC tissue microarrays and the TCGA-STAD dataset. Functional studies employed *H. pylori* (strain 49503)-infected GC cell lines and xenograft models, with autophagy manipulated by pharmacological induction, *Atg5* knockout, gene silencing, or overexpression. Molecular and cellular analyses included Western blotting, luciferase reporter assays, RNA sequencing, transmission electron microscopy (TEM), mitochondrial function tests, and additional functional assays. We observed elevated levels of LC3 and p-Drp1 in tumor tissues. *H. pylori* infection increased autophagy, cell migration, sphere formation, and transient tumor growth, while reducing cell viability and colony formation; autophagy induction suppressed these malignant features. TEM revealed abundant autophagy-like vesicles and mitochondrial alterations in infected cells. Mechanistically, *H. pylori* activated the Erk1/2 and JNK signaling pathways to induce autophagy while inhibiting other oncogenic signaling pathways. Notably, although *H. pylori* induces robust autophagy, further enhancement of this process using autophagy inducers attenuated gastric cancer malignancy, suggesting that further pharmacological modulation of autophagy warrants evaluation as a potential therapeutic strategy.

Keywords: Autophagy, *Helicobacter pylori*, gastric cancer

https://doi.org/10.62347/DUTL3079

Introduction

Autophagy is a fundamental cellular degradation pathway responsible for maintaining homeostasis by recycling damaged organelles and misfolded proteins. It plays a vital role in cellular responses to metabolic stress and nutrient deprivation. It is implicated in various human diseases, including cancer [1]. In the context of gastric cancer, *Helicobacter pylori* (*H. pylori*) infection is a well-established risk factor, especially in individuals with chronic gastritis or peptic ulcers [2-4]. Strains expressing the cytotoxin-associated gene A (CagA) are particularly associated with increased cancer risk [5]. Although autophagy is essential for cellular protection and immune regulation, its dysregulation during chronic *H. pylori* infection may promote bacterial persistence and carcinogenesis, indicating a complex role for autophagy in *H. pylori*-related gastric cancer [6-9].

Autophagy maintains cellular health by degrading and recycling intracellular components through lysosome-mediated pathways [1]. Over 30 autophagy-related genes (Atg), including *Atg5*, *Atg7*, and *Beclin-1*, are involved in this tightly regulated process [10]. One of the best-characterized autophagy markers is LC3, which is cleaved to form LC3-II, a component of autophagosome membranes that reflects autophagy activity [11]. Autophagy plays a dual role in cancer biology: it can suppress tumor initiation by preventing the accumulation of damaged proteins and organelles, but in established tumors, it may promote survival, metastasis, and drug resistance under metabolic stress [1, 12].

Phosphorylated Drp1 (p-Drp1) has been measured to quantify the activity of mitochondrial fission, a key process that regulates core cellular functions in cancer, including apoptosis, autophagy, and metastasis [13-15]. The activity of the Drp1 protein is tightly controlled by its phosphorylation state [16]. For example, phosphorylation at the Serine 616 (Ser616) site activates Drp1, thereby promoting mitochondrial fission, while phosphorylation at other sites, such as Serine 637 (Ser637), inhibits its activity [14, 15]. Therefore, measuring p-Drp1 levels can directly reflect the degree of mitochondrial fission and, in turn, help determine the state and fate of cancer cells. Mitochondrial fission is required to segregate damaged mitochondria for clearance via autophagy, particularly the selective process of mitophagy [15, 16]. In some cancers, enhanced mitochondrial fission is a mechanism that promotes autophagy, allowing cancer cells to survive under stress [17]. Drp1 phosphorylation is a downstream event of critical intracellular signaling pathways. Measuring changes in p-Drp1 helps to elucidate whether pathways such as AMPK or MAPK/ERK regulate mitochondrial dynamics to influence drug responses or the malignant progression of tumors [15, 18].

H. pylori is the most significant infectious contributor to gastric cancer, classified as a Group I carcinogen by the WHO. If left untreated, the infection induces chronic inflammation and can lead to atrophic gastritis and gastric adenocarcinoma [2-5, 19]. *H. pylori* infection in gastric cancer is tightly regulated by multiple molecular signaling pathways controlling autophagy. The Nod1-NF-κB/MAPK-ERK/FOXO4 pathway senses bacterial invasion, modulates autophagy-related proteins, and triggers inflammatory responses while suppressing autophagy and apoptosis [20]. The PI3K/Akt/mTOR pathway, particularly activated by the bacterial virulence factor CagA, inhibits autophagy by increasing mTOR activity [5]. The AMPK pathway promotes autophagy by inhibiting mTOR to maintain cellular energy balance. Additionally, the MAPK pathway, via JNK and ERK, exerts dual regulation where JNK induces autophagy and ERK can suppress it [21]. Bacterial factors such as VacA induce autophagy early during infection but later impair autophagy pathways, leading to substrate accumulation and DNA damage, which facilitate cancer progression. Gamma-glutamyltranspeptidase (HpGGT) disrupts lysosomal membrane integrity, further inhibiting autophagy and exacerbating chronic inflammation and tumorigenesis [22]. These intertwined signaling cascades and bacterial factors finely tune autophagy, influencing gastric cancer development and cell survival, and present potential therapeutic targets.

Autophagy also regulates the host defense against *H. pylori* through pathways such as NOD1, which activate innate immunity and facilitate bacterial clearance [23]. However, *H. pylori* counteracts these mechanisms by suppressing autophagic flux, allowing chronic colonization and increased cancer risk [24, 25]. Therefore, the dual roles of autophagy in pro-

moting both bacterial clearance and persistence make it a complex but promising target in gastric cancer prevention and therapy [22].

In gastric cancer, autophagy further contributes to chemotherapy resistance and immune escape. It regulates PD-L1 expression through the p62/SQSTM1-NF-κB pathway and can influence tumor dormancy and metastasis [26, 27]. Chemoresistance may also be mediated via ROS-NF-κB-HIF-1α signaling, and autophagy defects have been linked to altered metabolic phenotypes and tumor dissemination [26]. These findings suggest that autophagy modulators could be adjuncts to improve treatment outcomes. Compounds such as oleanolic acid and narciclasine have been shown to induce autophagy-dependent cell death via the PI3K/Akt/mTOR pathway [28, 29]. At the same time, miR-133a-3p and FOXP3 represent additional therapeutic targets within autophagy regulatory networks [30].

At the epigenetic level, histone modifications, including methylation and acetylation, play critical roles in gene expression and chromatin remodeling, influencing tumor biology [31-33]. Histone methylation, particularly of H3K9, has been implicated in cancer progression, with enzymes such as EHMT2 (G9a) emerging as crucial epigenetic regulators [34-36]. G9a catalyzes H3K9 methylation and represses transcription of autophagy-related genes such as Beclin-1, thereby reducing autophagic flux [37]. Inhibiting G9a reduces H3K9me2 levels, restores autophagy, promotes apoptosis, and suppresses tumor growth in various cancers, including gastric, pancreatic, and neuroblastoma [38-42].

In recent years, increasing attention has been directed toward the interplay between autophagy and cancer immunotherapy. Autophagy has been recognized as a critical regulator of tumor immunogenicity, antigen presentation, and immune checkpoint signaling, thereby influencing the efficacy of immune-based therapies. Notably, several recent studies published within the past two years have demonstrated that modulation of autophagy pathways can enhance responses to immune checkpoint blockade by reshaping the tumor immune microenvironment, promoting T cell activation, and improving antigen presentation [43-45]. These findings highlight autophagy as an emerging therapeutic target with the potential to synergize with immunotherapy and improve clinical outcomes across multiple cancer types.

These studies illustrate how *H. pylori* infection and epigenetic dysregulation converge on autophagy pathways, affecting tumor initiation, progression, immune evasion, and therapeutic responses. Understanding these interconnected processes may help identify novel therapeutic targets and improve clinical outcomes for gastric cancer patients.

While extensive research has elucidated the relationship between *H. pylori* infection and gastric cancer, the precise molecular mechanisms through which *H. pylori* regulates autophagy and how this contributes to carcinogenesis remain poorly understood [6, 20, 46-48]. Specifically, the dual role of autophagy as both a host defense and a bacterial survival mechanism introduces complexity that has yet to be fully unraveled. Moreover, although G9a-mediated epigenetic suppression of autophagy has been implicated in several cancers [37-42], its specific involvement in *H. pylori*-related gastric tumorigenesis remains unclear. There is also a lack of evidence on how therapeutic autophagy modulation, either activation or inhibition, can be optimally timed or targeted in *H. pylori*-associated gastric cancer. These knowledge gaps necessitate a more comprehensive understanding of the autophagy-epigenetics-infection axis.

To address the identified knowledge gap, this study investigated the molecular crosstalk among *H. pylori* infection, autophagy regulation, and gastric cancer development. The first step involves establishing *in vitro* gastric epithelial cell models of exposure to *H. pylori*. Autophagy flux was monitored, and CRISPR/Cas9 system was used to dissect the role of autophagy in modulating *H. pylori* infection-induced cellular changes. Parallel transcriptomic profiling (e.g., RNA-seq) was used to identify gene expression patterns by comparing wild-type and autophagy deficient cells with and without *H. pylori* infection. These datasets were integrated to explore how *H. pylori* modulates host autophagy to affect GC tumorigenesis. Finally, *in vivo* validation was conducted to determine the effects of autophagy modulation on tumor burden in the presence or absence of *H. pylori* infection.

Materials and methods

Cell lines and reagents

The human gastric epithelial cell line (GES-1) and the gastric adenocarcinoma cells (AGS and MKN45) were purchased from Bioresource Collection and Research Center (Hsinchu, Taiwan). Cells were maintained in the RPMI-1640 medium (HyClone, SH30027.01) with 10% fetal bovine serum (FBS, Gibco, 10437-028) and Pen/Step (100 Units/mL penicillin + 100 μg/mL Streptomycin, Gibco, 15140-122) at 37°C in a 5% CO_2 incubator. Amiodarone (AD; Sigma-Aldrich, A8423), an autophagy inducer, was purchased from Sigma, USA.

H. pylori strain and infection condition

The *H. pylori,* including standard strain ATCC 49503 (*Hp* 49503), was provided by Dr. Deng-Chyang Wu, Kaohsiung Medical University Hospital, Kaohsiung, Taiwan, and maintained on sheep blood agar. *H. pylori* was collected and resuspended in PBS. Cells (1×10^6) were seeded in a 6-cm dish without antibiotics overnight. Medium was replaced with serum- and antibiotics-free medium. Cells were infected with *H. pylori* at various multiplicities of infection in different experiments.

Cell transfection

Cells (2×10^5) seeded into a six-well plate were transfected with plasmid pATG5-EGFP (4 μg) by Lipofectamine™ 3000 following the manufacturer's instructions (Invitrogen, L3000015).

Immunoblotting analysis

The total protein from the cell lysate was collected from the cells after various treatments. For Western blotting, cells (1×10^6) were lysed in 100 μl of RIPA buffer. Lysates (30 μg protein) were electrophoretically separated by sodium dodecyl sulfate-polyacrylamide gel electrophoresis (SDS-PAGE) and transferred to a polyvinylidene difluoride (PVDF) membrane (Millipore, ISEQ85R). Membrane was blocked with 5% skimmed milk in PBST [sodium chloride (100 mM), disodium hydrogen phosphate (80 mM), sodium dihydrogen phosphate (20 mM), Tween 20 (0.2%), pH 7.5] for 1 h. The membrane was incubated with the primary antibody [LC3, 1:1000, MLB, PM036; EHMT2-G9A, 1:1000, abcam, ab185050; NF-κB p65, 1:1000, Cell Signaling, #8242; ATG5, 1:1000, abcam, ab108327; Phospho-NF-κB p65 (Ser536), 1:1000, Cell Signaling, #3033; p44/42 MAPK (Erk1/2), 1:1000, Cell Signaling, #4695; Phospho-p44/42 MAPK (Erk1/2) (Thr202/Tyr204), 1:1000, Cell Signaling, #4370; Stat3, 1:1000, Cell Signaling, #9139; Phospho-Stat3 (Tyr705), 1:1000, Cell Signaling, #9145; SAPK/JNK, 1:1000, Cell Signaling, #9252; Phospho-SAPK/JNK (Thr183/Tyr185), 1:1000, Cell signaling, #4668; PKA C-α, 1:1000, Cell signaling, #5842; GAPDH, 1:10000, GeneTex, GTX10-0118] at 4°C overnight. After washing with PBST, the membrane was hybridized with an HRP-conjugated secondary antibody (Thermo Fisher Scientific, 31460 and 31430) at RT for 1 h. The membrane was exposed to an imaging system to detect signals using chemiluminescence. Views were quantified by ImageJ software.

Immunofluorescent staining (IFA)

Cells (1×10^5/well) were seeded on a slide. Under different conditions, cells were then fixed in 4% formaldehyde for 20 min. The slide was incubated for 30 min in 0.1% Triton X-100 in PBS. The antibodies were added to the slide and left overnight at 4°C. The primary antibody (LC3; 1:50, MBL, M152-3) was visualized using an appropriate secondary antibody (Thermo Fisher Scientific, A11001). The fluorescent change of the cells was investigated under a confocal microscope (LSM 700; ZEISS). Views were quantified by ImageJ software.

CRISPR/Cas9-mediated gene editing

CRISPR/Cas9 RNP electroporation: GC AGS cells were synchronized with 200 ng/ml nocodazole for 17 h, followed by Cas9/gRNA delivery through electroporation. On the day of electroporation, an equal volume of cRNA and tracrRNA was mixed to prepare the gRNA complex solution (150 pmole). Cas9 protein (30 pmole) and 150 pmole gRNA were mixed in Opti-MEM™ I Reduced Serum Medium (ThermoFisher, #31985062) at RT for 15 min to form Cas9/gRNA ribonucleoprotein (RNP). At the same time, 1×10^5 of synchronized cells were collected by centrifugation and washed with Opti-MEM twice, then re-suspended in an optimal volume of Opti-MEM, followed by the addition of Cas9/gRNA RNP, which was deliv-

ered into the cell through NEPA21™ Electroporator. Gene editing efficiency was evaluated by T7E1 digestion and high-resolution melting (HRM) analysis. The electroporated cells were transferred immediately to a 24-well plate containing 1 ml of the corresponding culture medium and incubated in a 37°C, 5% CO_2 incubator. After 48 h of recovery, T7E1 and high-resolution melting were conducted to validate the gene editing efficiency. In addition, a limited dilution was carried out by seeding cells at a density of 1 cell/well. After two weeks of incubation, some single-cell clones were subjected to HRM-qPCR analysis to check the mutation in both target genes.

Transmission electron microscope investigation

Cells were washed with PBS, fixed with 2% paraformaldehyde (Sigma-Aldrich, 818715) and 2.5% glutaraldehyde (Sigma-Aldrich, 354-400) in 0.1 M PBS (pH 7.4) at 4°C for 24 h, followed by washing with 0.1 M PBS 3 times for 10 min. The samples were then treated with 2% aqueous osmium tetroxide (Sigma-Aldrich, 75633) in 0.1 M PBS at 4°C for 1.5 h, followed by washing 3 times with 0.1 M PBS for 10 min. Serial dehydration with different concentrations of ethanol (50-100%) (Merck, 102371) and washed with 1,2-propylene-oxide (Sigma-Aldrich, 807027) 2 times for 10 min. The samples were subsequently incubated in a 1:1 mixture of 1,2-propylene oxide and epoxy resin for 24 h. Finally, samples were embedded in Epoxy for 24 h. Ultrathin cell sections were then prepared, mounted on copper grids, and stained with 2% uranyl acetate and lead (II) citrate tribasic trihydrate (Sigma-Aldrich, 15326) for subsequent observation under a transmission electron microscope (TEM, HT7700, Hitachi High-Tech Corporation, Tokyo, Japan).

MTT assay

MTT solution (Sigma, M2128) (0.5 mg/ml in DMEM medium) was added to each well of the cells (4×10^3/well) in a 96-well plate after diverse treatments at 37°C for 3 h. The medium was replaced with 100 µl of DMSO (Sigma, D4540). Cell viability was determined by measuring the cell lysate at an optical density of 570 nm wavelength using a 96-well Multiskan™ Sky Microplate Spectrophotometer (Thermo Fisher Scientific).

Cell death analysis

Cells seeded in a 96-well plate underwent different treatments. At the end, 50 mL of the cultured medium was mixed with 50 µl reaction mixture of the Cytotoxicity Detection Kit (Roche, 11644793001) at RT for 10 min. Cells were cultured in a medium and treated with Triton X, which was the positive control for 100% cell death. The absorbance of the solution at 490 nm was measured using a Thermo Scientific™ Multiskan™ Sky Microplate Spectrophotometer.

Focus formation assay

Cells (1×10^3) in the 6 cm culture dish received different treatments for 7 days to allow colony formation. These cells were then fixed with 4% formaldehyde and stained with 0.4% crystal violet (Sigma, V5265), followed by lysis with 2% SDS solution. Measurements were done at an optical density of 570 nm wavelength using a 96-well Multiskan™ Sky Microplate Spectrophotometer (Thermo Scientific).

Tumor sphere formation assay

AGS cells (5×10^3 cell) in the 6-well culture-plate received different treatments and were maintained in DMEM/F12 serum-free medium together with 1× B27 supplement (Gibco, 17504044), 20 ng/mL bFGF (Gibco, 100-18B-50UG) and 20 ng/mL EGF (Sigma, E4127). The suspended cells were collected and maintained in the ultra-low attachment 6-well plates (Corning, 3471). Cells formed tumor spheres after 7 days, and the number of tumor spheres was counted when the sphere diameter was greater than 50 µm.

Wound healing assay

Cells (8×10^5) were seeded in a 2-well culture insert, which was placed in a 12-well plate. The insert was removed after the cell monolayer was formed. Cells were treated with/without amiodarone, followed by *H. pylori* infection at MOI of 50 or 75 under serum starvation for 24 h. Each well was washed with 1× PBS to remove residual cell debris. The wound healing was observed under a light microscope. Images were quantified by ImageJ software.

Transwell™ migration assay

A Transwell™ insert with a Millipore membrane (pore size of 8 µm, Corning, 3422) was used.

Initially, cells (5×10^4/well) after treatment with 5 μM AD for 3 h and *H. pylori* (MOI=75) infection for 24 h were seeded in the upper chamber with 0.1 ml serum-free medium. Normal medium with 10% FBS was added to the lower chamber as a chemoattractant. Cells were incubated for 72 h. The cells attached to the reverse side of the membrane were then fixed and stained. Five random views were photographed under an inverted microscope and quantified using ImageJ software.

Cell mito stress test

The mitochondrial function of AGS cells with or without *H. pylori* infection was measured by a Seahorse XF HS Mini Analyzer (Agilent). A Seahorse XFp Cell Mito Stress Test Kit (103010-100, Seahorse Bioscience) was used to evaluate the mitochondrial metabolism according to the manufacturer's instructions.

ROS assay

AGS cells (5×10^5) were cultured in a 6-well plate and allowed to stabilize for 24 h at 37°C under 5% CO_2. Then ROS was stained using ROS-ID™ total ROS detection kit according to the manufacturer's protocol (ENZ-51011, Enzo Life Sciences). Finally, the Attune NxT Flow Cytometer (Thermo Fisher Scientific Inc.) was used to count cells for verification.

Tissue microarray (TMA) of GC specimens

A total of 11 tissue array slides of human gastric cancer specimen sections provided by Dr. Deng-Chyang Wu (KMUH, Kaohsiung, Taiwan) were analyzed. The study was conducted according to the guidelines of the Declaration of Helsinki and approved by the Ethics Committee of the Institutional Review Board of Kaohsiung Medical University Hospital (KMUH-IRB-20120176). These tissue array slides contained one hundred sixty paired paraffin-embedded GC specimens at various stages.

Immunohistochemical staining (IHC) of the GC specimens in the tissue array

Immunohistochemistry (IHC) was performed on 4-μm-thick formalin-fixed paraffin-embedded sections. Polyclonal rabbit anti-LC3 antibody (1:300, MBL, PM036), anti-p-Drp1 (1:50, Bioss antibodies, bs-12702R), and anti-Ki-67 antibody (1:250, Sigma-Aldrich, AB9260) were used as the primary antibodies. The procedures followed the protocol of the Bond-Max Automated IHC stainer (Leica Biosystems Newcastle Ltd., Australia). Briefly, tissues were deparaffinized with xylene and pre-treated with the Epitope Retrieval Solution 1 (ER1) (citrate, pH 6.0, 100°C, 20 min) followed by incubation with the primary antibody at RT for 30 min. Subsequently, the tissues were incubated with polymer for 15 min, followed by hydroperoxide blocking for 5 min. Tissues were then developed with 3,3'-diaminobenzidine chromogen for 10 min using the Bond Polymer Refine Detection Kit (Leica Biosystems Newcastle Ltd, United Kingdom). Finally, the tissues were counterstained with hematoxylin for 5 min.

TMA scoring

LC3 IHC staining of the tissue sections was scored based on staining intensity and the percentage of positive cells. The staining intensity was scored as follows: 0, no dots or barely visible dots in <5% of the cells; 1, detectable dots in 5-25% of cells; 2, readily detectable dots in 25-75% of cells; 3, dots in >75% of cells [49]. Percentages ≤10, 11-25, 26-50, 51-75, and ≥75% were scored as 0, 1, 2, 3, and 4, respectively, for p-Drp1 (S616). Non-significant brown (absent), slight brown (weak), moderate brown (moderate), and deep brown (strong) staining intensities were scored as 0, 1, 2, and 3, respectively [50]. A total immune reactive staining score was then obtained by multiplying the intensity and extension scores, ranging from 0 to 12 for p-Drp1. Stained tissues were analyzed under a light microscope and estimated by an experienced pathologist.

TCGA database and UALCAN bioinformatic analysis of gene expression

The gene expression data sets for STAD (stomach adenocarcinoma) and adjacent normal tissue were obtained from The Cancer Genome Atlas (TCGA) database, containing 415 carcinoma and 34 normal samples. UALCAN portal analysis (http://ualcan.path.uab.edu/index.html) of STAD samples was from the TCGA database. Differential gene expression between normal and tumor gastric cancer specimens was compared.

Xenograft gastric cancer nude mouse model

Male nude mice (5 weeks old) were obtained from the National Laboratory Animal Center, Taipei, Taiwan. The mice were maintained in a pathogen-free facility under isothermal conditions with regular photoperiods in the KMU Center for Laboratory Animals. The experimental protocol adhered to the regulations of the Animal Protection Act of Taiwan and was approved by the Institutional Animal Care and Use Committee (IACUC) of the university (Affidavit of Approval of Animal Use Protocol No. 108186). Mice (n=42, 7 weeks old) were randomly divided into six groups: (i) AGS cells (n=4); (ii) AGS cells plus *Hp* 49503 (n=8); (iii) AGS cells plus AD (autophagy inducer) (n=4); (iv) AGS cells plus *Hp* 49503 plus AD (n=8); (v) AGS-R1 cells (*Atg5-/-*) (n=4); (vi) AGS-R1 cells plus *Hp* 49503 (n=8). In this xenograft mouse model, male nude mice (7 weeks) were inoculated with cells (2×10^6 cells in 100 µl of PBS) subcutaneously on the back of the mice. The tumor volume was measured according to the following formula: Tumor volume (mm^3) = length (mm) × width^2 (mm^2) ×0.5. Body weight and tumor size were measured weekly until the end of the experiment.

Statistical analysis

All experiments were analyzed using GraphPad Prism ver. 10.3.1 (GraphPad Software, Inc., San Diego, CA, USA). Data were analyzed using Student's t-tests, Chi-square test, Fisher's exact test, or one-way ANOVA with Tukey's multiple comparison test. Statistical significance is represented as *: $P<0.05$; **: $P<0.01$; ***: $P<0.001$. All experiments were repeated at least three times, and all values were presented as mean ± SD.

Results

The expression level of autophagy and mitochondria fission markers in clinical GC specimens and TCGA STAD database

To determine the status of autophagy activity and mitochondria function in GC patient, GC specimens (tumor and adjacent non-tumor tissues) were analyzed. One hundred and sixty paired GC patient specimens at various clinical stages were obtained from the tissue array of KMU hospital, Kaohsiung, Taiwan (Table S1). The expression levels of autophagy marker "LC3" and mitochondria fission marker "phosphorylated Drp-1 (p-Drp1)" were assessed by immunohistochemical (IHC) staining. LC3 and p-Drp1 expression levels were scored based on previously published methods [49, 50].

Our data showed that GC patient specimens, either total tumors or from stage I to IV, showed higher levels of autophagy LC3 and p-Drp1 compared to the adjacent normal tissues of GC specimens in the tissue array (**Figure 1A** and **1B**). We further analyzed the TCGA database of gastric cancer (STAD), and found that higher levels of MAP1LC3B (LC3) and DNM1L (Drp1) mRNA in tumor tissues as compared to non-tumor parts (**Figure 1C**). These findings indicate that high autophagy activity and mitochondria dysfunction occurred in GC tumor tissues. To further explore the clinical relevance, we conducted a multivariate analysis to assess the associations of LC3 and p-Drp1 protein levels with clinicopathological characteristics in GC patients. Patients were divided into high-risk and low-risk groups based on marker expression levels, followed by Fisher's exact test analysis. No significant associations were found among the expression levels of LC3, p-Drp1 and clinicopathological parameters, including gender, age, tumor size, lymphatic/vascular invasion, nerve invasion, or TNM stage (**Table 1**), which may suggest a role for metabolic adaptation and mitochondrial dysfunction in GC tumor cell survival.

The expression of G9a, LC3, and p-Drp1 in gastric as well as GC cells co-cultured with H. pylori

G9a, a histone methyltransferase, regulates DNA methylation and chromatin remodeling and plays critical roles in tumor cell proliferation, apoptosis, differentiation, and drug resistance [51]. Notably, G9a acts as a negative regulator of autophagy through mTOR activation or Beclin-1 suppression and is frequently overexpressed in various cancers, including gastric cancer [51]. Due to its oncogenic properties, G9a has emerged as a promising therapeutic target [52].

To investigate the effects of *H. pylori* on autophagy and mitochondria function, we infected normal gastric epithelial GES-1 and gastric cancer AGS and MKN45 cell lines with *H. pylori*

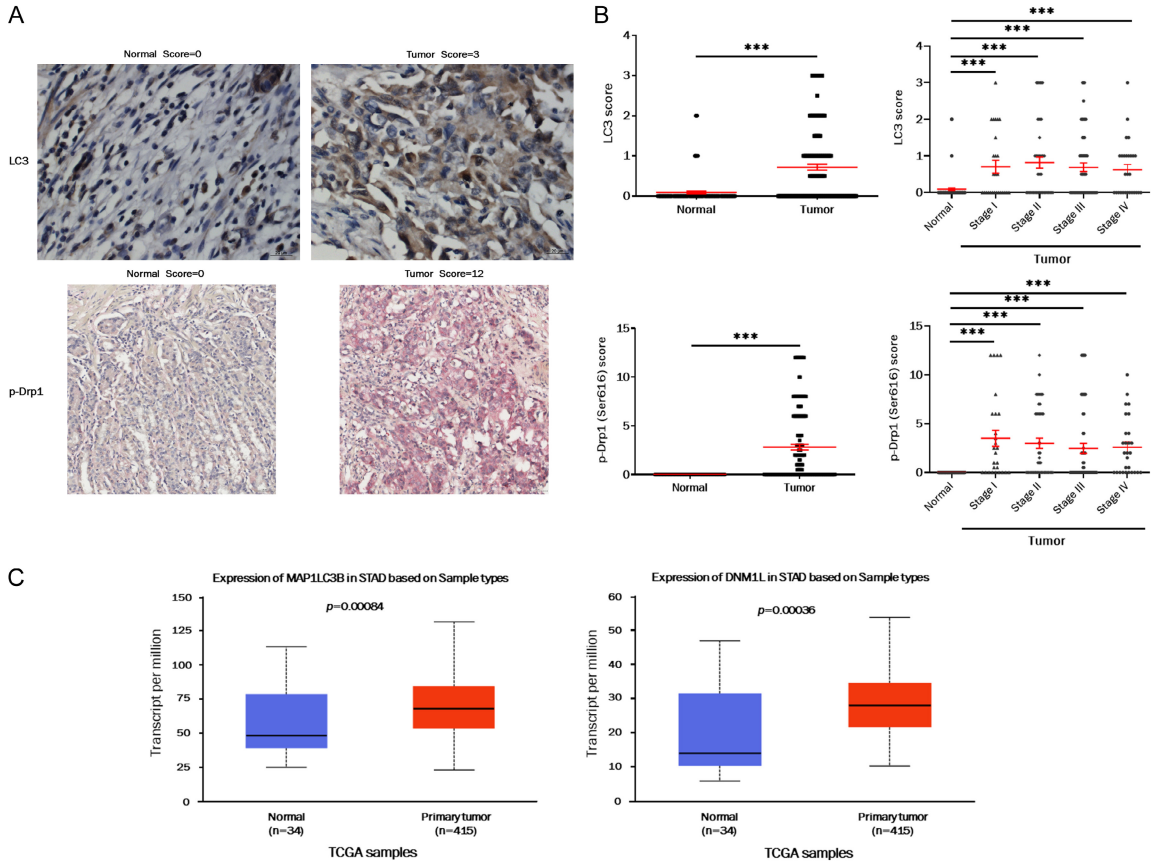

Figure 1. The expression level of LC3 and p-Drp1 in clinical GC specimens and the TCGA STAD database. A. A representative image to show LC3 and p-Drp1 protein expression in the GC specimen tumor part vs. LC3 protein expression in the adjacent normal tissue in the tissue array sections. Scale bar =20 um (LC3)/50 um (p-Drp1). B. Quantification of LC3 and p-Drp1 protein levels in tumor vs. non-tumor and non-tumor vs. various stages in 160 GC specimens. Pathologists classified expression levels based on a score of 0 to +3 for LC3 and 0 to +12 for p-Drp1. Error bars represent mean ± SEM. Data were analyzed using Student's t-test or one-way ANOVA. ***: P<0.001. C. Quantification of MAP1LC3B and DNM1L mRNA levels in normal (n=34) and primary tumor (n=415) tissues using TCGA STAD database by box-whisker plots.

strain *Hp* 49503 ($CagA^+/VacA^+$, ATCC 49503) at the multiplicity of infection (MOI) of 75, 100, and 150. After 24 h of infection, we evaluated protein levels of G9a, the autophagy LC3, and the mitochondria fission protein p-Drp1 via Western blotting. We further assessed LC3 puncta number, intensity of p-Drp1, and the subcellular localization of p-Drp1 in AGS cells under immunofluorescence microscopy. Western blot analysis revealed that *H. pylori* infection increased LC3-II levels while decreasing G9a and p-Drp1 expression in three MOI titers across all three gastric cell lines (**Figure 2A-C**). Consistently, AGS cells co-cultured with *H. pylori* displayed increased LC3 puncta, but reduced intensity of p-Drp1 and no evident colocalization with LC3 under confocal microscopy (**Figure 2D**), suggesting that *H. pylori* infection independently induces autophagy and abrogates mitochondria fission.

We further investigated the mitochondria respiration rate of AGS cells with or without *H. pylori* infection. AGS cells infected with *H. pylori* (MOI=25) exhibited increased basal and maximal mitochondrial respiration by Seahorse mitochondrial stress test (**Figure 2E**). Due to high toxicity of *H. pylori*, only low MOI (25) of *H. pylori* can yield consistent results. The results imply that *H. pylori* infection induces the mitochondria to produce more ATP and induce overall metabolic activity. This increase suggests the mitochondria have a greater potential to generate energy, which indicates a compensatory mechanism or a heightened energy demand. We further measured the intracellular

Table 1. Correlation of tissue LC3 and p-Drp1 protein levels with clinicopathologic parameters of GC patients

Expression pattern	Gender	Age	Tumor size	Lymphatic or vascular invasion	Nerve invasion	Stage
LC3†	0.3193	0.1487	0.7796	0.3457	0.9958	0.2338
p-Drp1†	0.8167	0.3556	0.4982	0.172	0.6259	0.8494
LC3 & p-Drp1‡	0.4125	0.7851	0.1799	0.4271	0.2904	0.5916

1. All the numbers represent *P* values. 2. High protein expression was defined as greater than the average level in the tumor tissue. The definition of gender, age, tumor size, lymphatic or vascular invasion, nerve invasion, and stage are the same as in Table S1. †Single-factor analysis was conducted using the two-tailed Student's t-test. Results were obtained by measuring the levels of LC3 and p-Drp1 protein after IHC staining in the tissue array. ‡Fisher's exact test was used for the multiple factor analysis, by which high LC3 and high p-Drp1 expression were defined as the high-risk group, as shown in **Figure 1**. This method compared the relationship between high-risk and low-risk groups.

ROS production of AGS cells with or without *H. pylori* infection by flow cytometry analysis. In the control group, 9.15% of ROS-positive (ROS-FITC+/+) cells were detected. As a positive control, ROS-positive AGS cells with H_2O_2 treatment markedly increased to 20.34%. Notably, AGS cells co-cultured with *H. pylori* (MOI=25) resulted in an elevation of ROS percentage (13.61%) compared to the control. Co-treatment with the antioxidant N-acetylcysteine (NAC) reversed the ROS elevation to 8.95% in *H. pylori* + NAC group, comparable to the baseline level (**Figure 2F**). While increased respiration rate might seem positive for energy production (**Figure 2E**), the simultaneous increase in ROS (**Figure 2F**) suggests that this increased activity leads to oxidative stress. ROS are byproducts of mitochondrial respiration, and their overproduction can damage cellular components, including the mitochondria themselves [53].

In summary, *H. pylori* infection in GC cell lines disrupts normal mitochondria function and suppresses G9a expression while promoting autophagy. The absence of colocalization between LC3 and p-Drp1 further indicates functional uncoupling of autophagy activity and mitochondria.

H. pylori infection activates MAPK and NF-κB signaling pathways to regulate autophagy in GC cells

To determine signaling pathways related to *H. pylori* infection and autophagy activation in gastric cancer cells, we either enhanced autophagy activity using the inducer–or knocking out the *Atg5* gene via CRISPR-Cas9 system. We established the stable Atg5 knockout clones including a heterozygous Atg5 knockout clone AGS-C19 and a homozygous knockout clone AGS-R1 confirmed by genome sequencing. We demonstrated that AGS-R1 did not show Atg5 protein expression (Figure S1A) and had fewer green puncta number than wild-type AGS cells in the presence of *H. pylori* (Figure S1B). We then examined whether the H. pylori infection and induction of autophagy activity affect G9a, autophagy LC3-II and mitochondria p-Drp1 protein levels at 24 h post-infection. Our data showed that the *H. pylori* infection resulted in suppression of G9a, Drp1, p-Drp1, and cyclin D1 (**Figure 3A** and **3B**). Notably, LC3-II level was increased in *H. pylori*-infected AGS and MKN45 cells compared to uninfected controls (**Figure 3A**, lanes 2 and 3 vs. lane 1; **Figure 3B**, lane 2 vs. lane 1). Moreover, G9a, Drp1, p-Drp1, and cyclin D1 were not affected by amiodarone-induced autophagy in two cell lines (**Figure 3A** and **3B**). To further investigate whether *H. pylori* infection induces an autophagic degradation process, AGS and MKN45 cells were pretreated with the autophagosome-lysosome fusion blocker "CQ" (50 μM) for 3 h, followed by co-culture with *H. pylori* for an additional 24 h. The results showed that LC3-II accumulation was slightly increased in *H. pylori*-infected cells in the presence of CQ (**Figure 3A**, lane 3 vs. 7; **Figure 3B**, lane 2 vs. 6), indicating that *H. pylori* infection modulates autophagy degradation processes. However, the levels of G9a, p-Drp1and cyclin D1 remained unchanged. In addition, c-Myc protein expression was also suppressed by *H. pylori* in MKN45 cells; however, it is undetectable in AGS cells (**Figure 3B**). We further used AGS-R1 cells (*Atg5-/-*) to validate the effect of autophagy on *H. pylori* infection-related molecules in gastric cancer cells. We found that the suppression of G9a, p-Drp1 and cyclin D1 by *H. pylori* was not affected in this *Atg5* knockout cell line (**Figure**

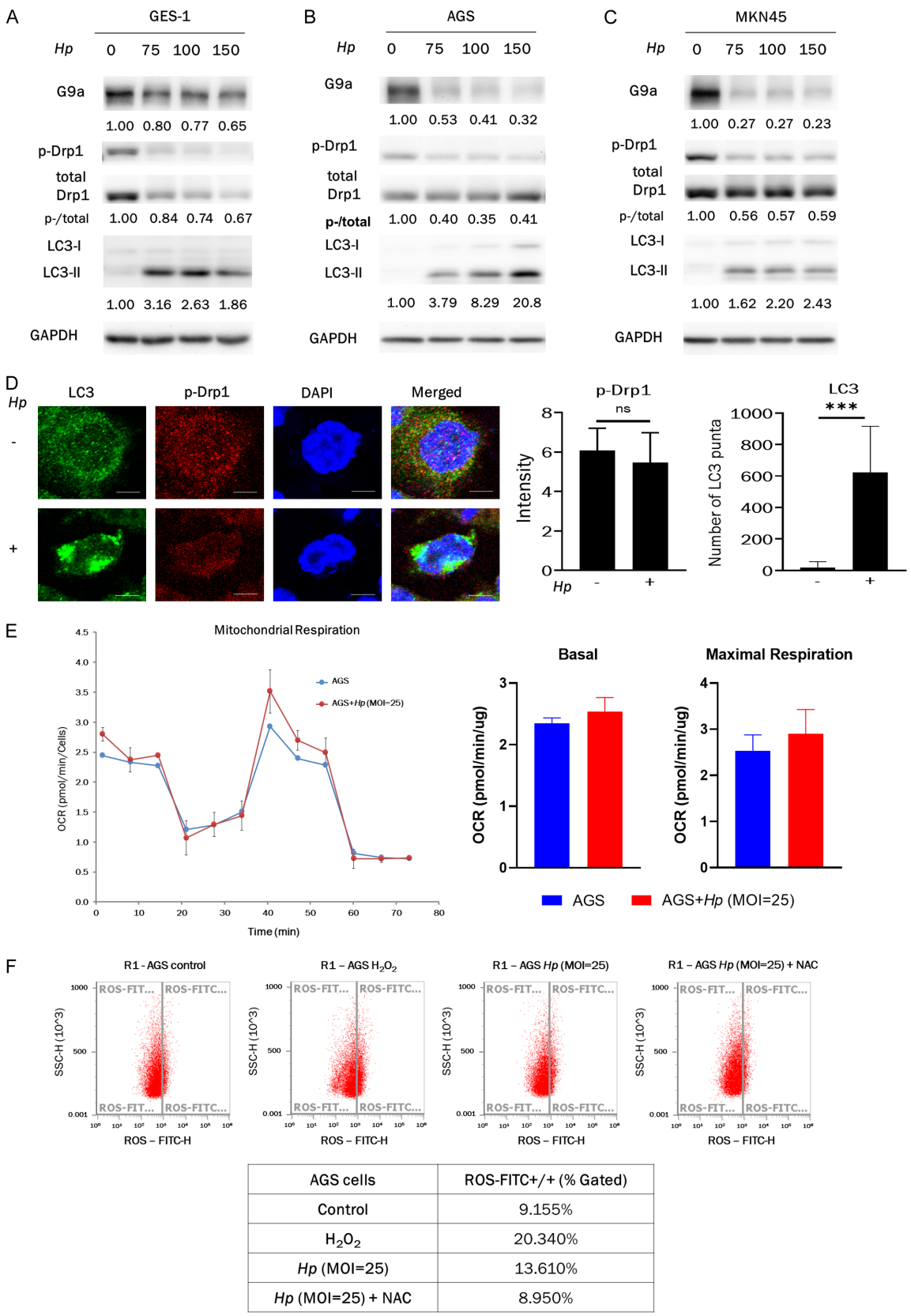

AGS cells	ROS-FITC+/+ (% Gated)
Control	9.155%
H_2O_2	20.340%
Hp (MOI=25)	13.610%
Hp (MOI=25) + NAC	8.950%

Figure 2. The expression of G9a, LC3, and p-Drp1 in gastric and GC cells co-cultured with *H. pylori*. (A) GES-1 and (B) AGS (C) MKN45 were co-cultured with or without *H. pylori* at the MOI of 75, 100, and 150 for 24 h. Protein expres-

sion was detected by Western blotting using specific antibodies. GAPDH was used as the internal control. (D) AGS cells with or without *H. pylori* treatment for 24 h was labelled with specific antibodies and visualized under a confocal fluorescent microscope. Scale bar =10 μm. Error bars represent mean ± SD of three independent experiments. Data were analyzed by Student's t-test. ns: no significant; ns: no significant; *: $P<0.05$; **: $P<0.01$; ***: $P<0.001$. (E) Seahorse mitochondrial Stress Test in the normal and *H. pylori*-infected groups. The left side shows the Oxygen Consumption Rate (OCR) profile plot, and the right shows basal and maximal respiration. (F) Flow cytometric analysis of intracellular ROS production in AGS cells revealed differential effects among treatment groups.

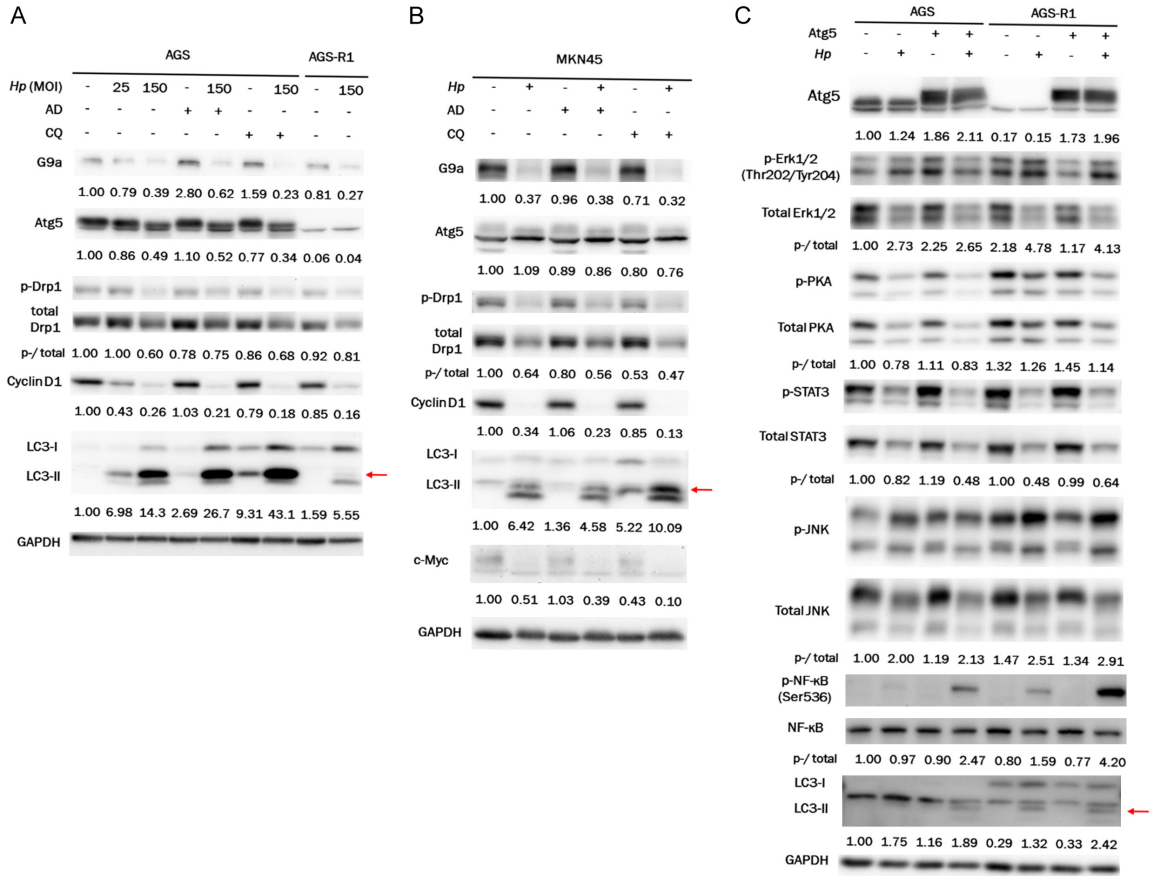

Figure 3. Effect of autophagy, mitophagy, and related signaling pathways on *H. pylori*-infected GC cells by manipulating the autophagy activity. For induction of autophagy activity, (A) AGS and (B) MKN45 cells were treated with the inducer AD (5 μM) for 3 h and the medium was replaced with fresh medium containing or not containing *Hp* 49503 (MOI=150) for another 24 h. GC cells were pretreated with CQ (50 μM) for 3 h, then co-cultured with *Hp* 49503 for 24 h. For suppression of autophagy activity, the *Atg5* gene level was suppressed using CRISPR/Cas9 knockout *Atg5* gene together with *Hp* 49503 infection for another 24 h in AGS cells. (C) AGS and AGS-R1 were co-cultured with or without *Hp* 49503 at the MOI of 150 for 24 h. ATG5 plasmid DNA was transiently transfected into the AGS and AGS-R1 cells. The expression level of ATG5 protein in these transfected cells was measured using an anti-ATG5 antibody by immunoblotting. Other protein markers were detected by Western blotting using specific antibodies. GAPDH was used as the internal control.

3A, lane 3 vs. 9). Altogether, above findings are consistent with the notion that *H. pylori* simultaneously induces autophagy, disrupts mitochondrial fission as well as the expression of G9a and cyclin D1 via a mechanism independent of *Atg5*-related autophagy.

To further clarify *H. pylori* infection-related signaling pathways affected by autophagy in GC cells, two sets of RNA-seq data were analyzed using wild-type AGS and *Atg5* knockout AGS-R1 cells, with or without *H. pylori* infection, and were analyzed by the Cufflinks suite. Differentially Expressed Genes (DEG) were determined by [$\log_2$ fold change] ≥1 and *p*-value <0.05. The identified DEGs were subjected to KEGG pathway enrichment analysis to map gene expression networks. Comparing the

DEGs of AGS + *H. pylori* with the AGS control, twenty-one signaling pathways were significantly enriched (Figure S2). Among them, mitophagy (hsa04137), Wnt (hsa04310), MAPK (hsa04010), and PI3K-Akt (hsa04151) pathways-related to autophagy signaling transduction were identified in AGS + *H. pylori* but not in AGS-R1 + *H. pylori* (data not shown). To validate the relationship between autophagy and these signaling pathways, we used either knockout or overexpressing *Atg5* gene in AGS cells with or without *H. pylori*. In wild-type AGS cells, we observed that *H. pylori* infection reduced levels of total Erk1/2, p-PKA, total PKA, p-STAT3, total STAT3, and total JNK, but elevated levels of p-Erk1/2, p-JNK, p-NF-κB, and LC3-II (**Figure 3C**, lane 2). These data imply that *H. pylori* infection upregulates proliferation and stress markers (p-Erk1/2 and p-JNK), proinflammatory immune cell marker (p-NF-κB), as well as the autophagy marker LC3-II. Furthermore, in *Atg5* knockout AGS-R1 cells, *H. pylori*-induced p-Erk1/2, p-PKA, p-NF-κB, and p-JNK were further boosted compared to wild-type AGS cells (**Figure 3C**, lane 2 vs. lane 6). However, overexpression of Atg5 did not significantly alter *H. pylori*-related signaling pathways in either AGS-WT or AGS-R1 cells, except p-NF-κB (**Figure 3C**; lane 2 vs. lane 4, and lane 6 vs, lane 8). These data suggest that loss of autophagy slightly enhances the pro-survival, metabolic, and stress-related signaling pathways (Erk1/2, JNK, PKA, NF-κB, and JNK).

We further used PathDetect™ trans-reporting systems (Agilent) to validate the relationships among *H. pylori,* autophagy, and related signaling pathways. A total of 6 luciferase reporter systems were screened in the presence or absence of *H. pylori* (MOI=150) infection with or without induction of autophagy. Our data showed that *H. pylori* infection significantly upregulated NF-κB, Erk1/2 (ELK1), and c-Jun (JNK) signaling pathways (Figure S3). However, increasing autophagy activity did not seem to affect *H. pylori*-upregulated signaling pathways (Figure S3). This finding is consistent with the Western blot result of **Figure 3C**.

Taken together, *H. pylori* infection decreases the expression of c-Myc, G9a, p-Drp1, cyclin D1, p-PKA, and p-STAT3, while increasing levels of p-Erk1/2, p-JNK, p-NF-κB, and LC3-II. Although *H. pylori* alters multiple signaling cascades, and some pathways are autophagy-sensitive (such as Mitophagy, Wnt, MAPK, PI3K-Akt) (Figure S2), autophagy seems to have no evident influence on *H. pylori*-related signaling pathways. Moreover, p-Drp1 is suppressed by *H. pylori* infection but not autophagy deficiency (**Figure 3A**). These findings suggest that G9a and the mitochondria fission marker p-Drp1 are suppressed by *H. pylori* in an autophagy-independent manner, and *H. pylori* infection induced autophagy in a G9a-independent manner.

In summary, *H. pylori* triggers two MAPK signaling axes (Erk and JNK) to induce autophagy while disrupting mitochondrial fission and possibly resulting in mitophagy.

The ultrastructure of AGS and AGS-R1 cells with and without H. pylori infection under transmission electron microscopy

Transmission electron microscopy (TEM) analysis revealed more *H. pylori* within infected AGS cells than AGS-R1 cells and uninfected controls (**Figure 4A** and **4B**). Numerous rod-shaped *H. pylori* were also observed outside the AGS cell membranes (**Figure 4C** and **4D**, white arrow). Notably, rod-like bacteria particles were detected closely adhered to the cell membrane, as indicated by white arrows (**Figure 4C**). Moreover, *H. pylori* particles were also detected within the single-membrane autophagic-like vesicles (V) in AGS cells and cytoplasm of AGS-R1 cells (**Figure 4C** and **4D**, white arrow head). In contrast, very few autophagic-like vesicles were in AGS-R1 cells co-cultured with *H. pylori* (**Figure 4D**). These ultrastructural vesicles suggest that *H. pylori*-induced autophagic-like vesicles may facilitate *H. pylori* replication in wild-type AGS cells. Moreover, we also observed mitochondria with abnormal morphology in infected AGS and AGS-R1 cells (**Figure 4C** and **4D**, M), which is consistent with *H. pylori*-related suppression of p-Drp1.

Effect of autophagy on the viability, focus formation, migration, and sphere formation of AGS and AGS-R1 cells with or without H. pylori infection

Initially, we investigated whether modulation of autophagy affects AGS cell viability in the presence of *H. pylori*. Autophagy was manipulated using the autophagy inducer (AD) or *Atg5* gene knockout system, and cell viability was assessed by MTT assay. AGS cells were infect-

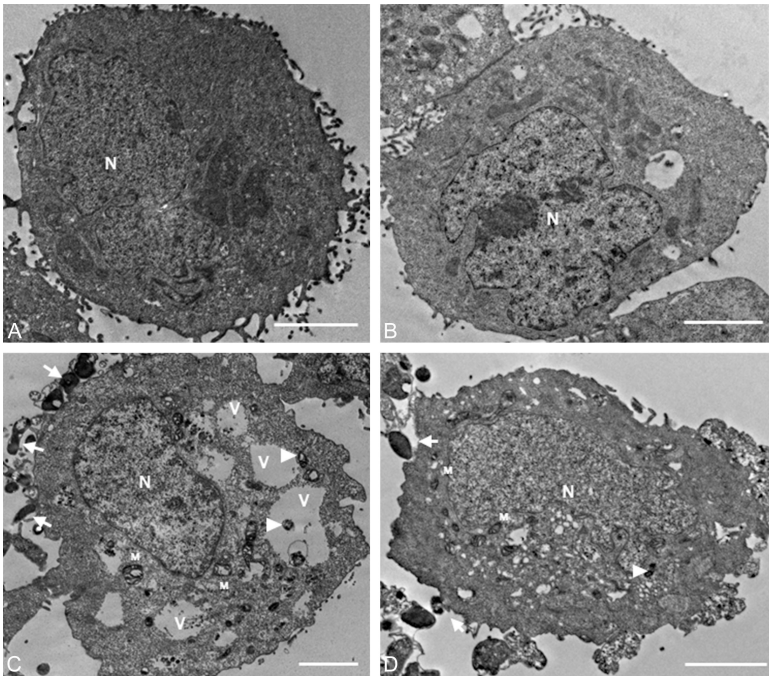

Figure 4. The ultrastructure of AGS and AGS-R1 cells with and without *H. pylori* infection under transmission electron microscopy. TEM investigation of the ultrastructure of the uninfected (A) AGS and (B) AGS-R1 cells without infection, and (C) AGS and (D) AGS-R1 cells were co-cultured with *H. pylori* (MOI=150) for 24 h. Adherent (white arrow) and internalized (white arrowhead) *H. pylori* are shown. Scale bar =2.5 μm. N: nucleus; V: autophagic-like vesicle; M: mitochondria.

ed with *H. pylori* at MOI of 150. Our data showed an evident reduction in AGS cell viability upon *H. pylori* infection compared to uninfected controls (**Figure 5A**, columns 1 vs. 2). Autophagy induction by AD further decreased the viability of *H. pylori*-infected AGS cells (**Figure 5A**, column 2 vs. 4). In contrast, AGS-R1 cells (*Atg5* knockout) exhibited only a slight reduction in the viability with or without *H. pylori* infection compared to wild-type AGS cells (**Figure 5A**, columns 1 and 2 vs. 5 and 6). Lactate dehydrogenase (LDH) cytotoxicity assay showed that *H. pylori* infection results in significant cytotoxicity in AGS and AGS-R1 cells (**Figure 5B**, columns 2 and 6). In contrast, AD treatment resulted in minimal cytotoxic effect (**Figure 5B**, column 3). These results suggest that *H. pylori* infection reduces AGS cell viability, and enhanced autophagy further exacerbates this reduction.

We then performed the focus formation assay to assess the impact of autophagy on other malignant transformation features, which measures cancer cells loss of contact inhibition. *H. pylori* (MOI=150) significantly reduced focus formation in AGS cells (**Figure 5C**, columns 1 vs. 2). Autophagy induction further suppressed the number of foci in the presence of *H. pylori* (**Figure 5C**, column 2 vs. 4). *H. pylori* suppression of focus formation resulted in no evident change in AGS-R1 cells (**Figure 5C**, column 2 vs. 6). These findings, consistent with the MTT results in **Figure 5A**, indicate that *H. pylori* infection suppresses colony formation in AGS cells, and this suppression is exacerbated by enhanced autophagy.

We next examined the impact of *H. pylori* infection on cell migration. Infection of three GC cell lines with *H. pylori* at MOI of 50 and 75 showed significant increase of their motility in a dose-dependent manner (Figure S4A and S4B), whereas MKN45 cells showed reduced migration upon *H. pylori* infection (Figure S4C). In AGS cells, pretreatment with AD for 3 h followed by *H. pylori* infection demonstrated that while *H. pylori* increased cell motility, autophagy induction reduced it. In addition, *Atg5* knockout did not affect cell migration (**Figure 5D**). Similarly, Transwell™ assays showed that *H. pylori*-infected (MOI=75) AGS cells migrated faster than uninfected controls, and autophagy activation significantly suppressed this migration. This effect was abolished in *Atg5* knockout cells (**Figure 5E**). These results suggest that *H. pylori*-induced motility is suppressed by autophagy activation.

Finally, we explored the effect of *H. pylori* infection and autophagy on tumor-sphere formation, a stemness marker. AGS cells were infected with *H. pylori* (MOI=25) under non-adherent culture conditions. Tumor-sphere formation was significantly increased after *H. pylori* infection (**Figure 5F**, column 1 vs. 2). Induction of autophagy by AD suppressed sphere formation (**Figure 5F**, columns 2 vs. 4). AGS-R1 cells formed fewer tumor-spheres than wild-type AGS cells, regard-

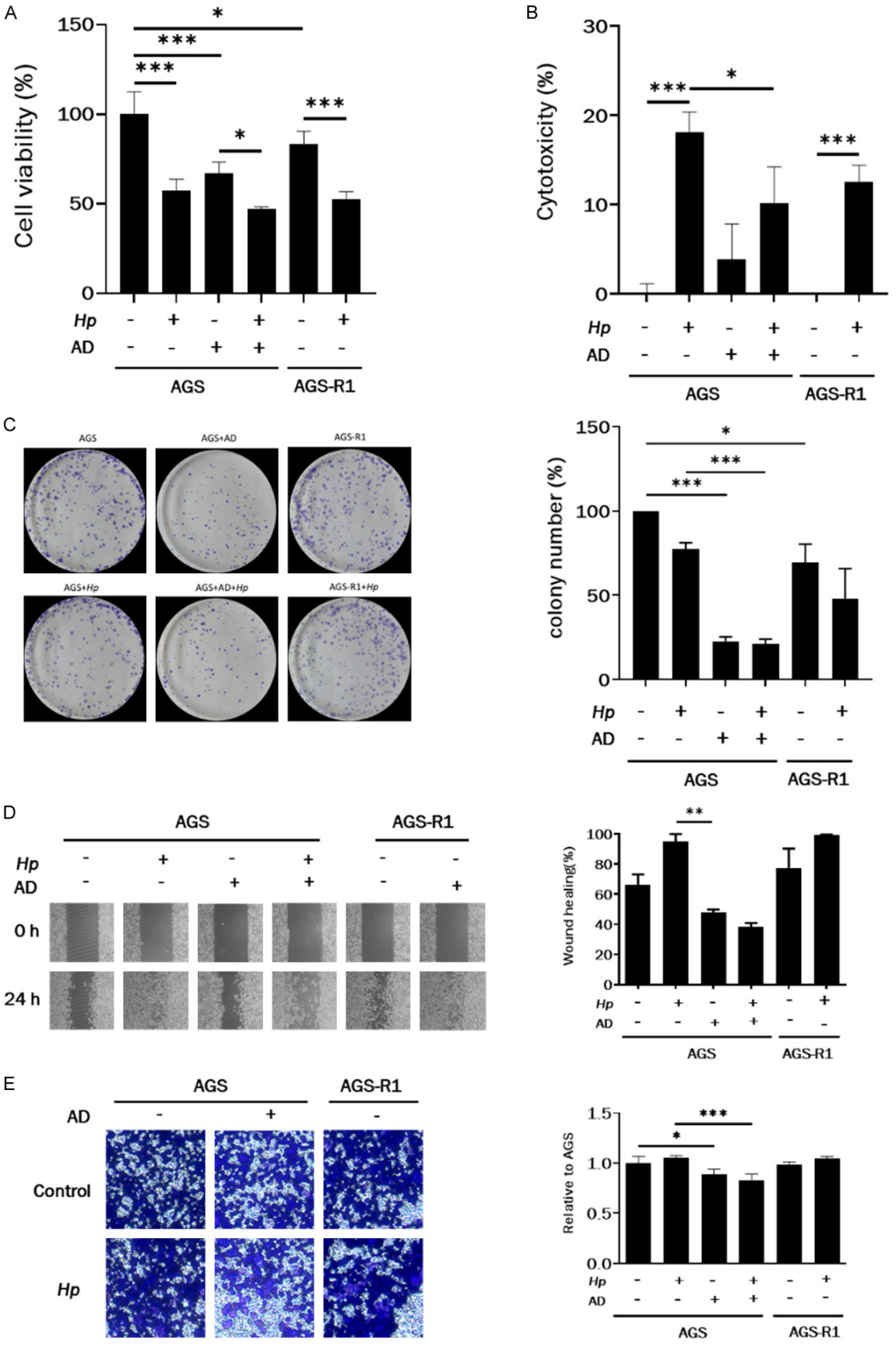
A
Cell viability (%)
150
100
50
0
*
***
***
*
***
Hp - + - + - +
AD - - + + - -
AGS
AGS-R1
B
Cytotoxicity (%)
30
20
10
0
***
*
***
Hp - + - + - +
AD - - + + - -
AGS
AGS-R1
C
AGS
AGS+AD
AGS-R1
AGS+Hp
AGS+AD+Hp
AGS-R1+Hp
colony number (%)
150
100
50
0
*
***
***
Hp - + - + - +
AD - - + + - -
AGS
AGS-R1
D
AGS
AGS-R1
Hp - + - + - -
AD - - + + - +
0 h
24 h
Wound healing(%)
100
80
60
40
20
0
**
Hp - + - + - +
AD - - + + - -
AGS
AGS-R1
E
AGS
AGS-R1
AD - + -
Control
Hp
Relative to AGS
1.5
1.0
0.5
0.0
***
*
Hp - + - + - +
AD - - + + - -
AGS
AGS-R1

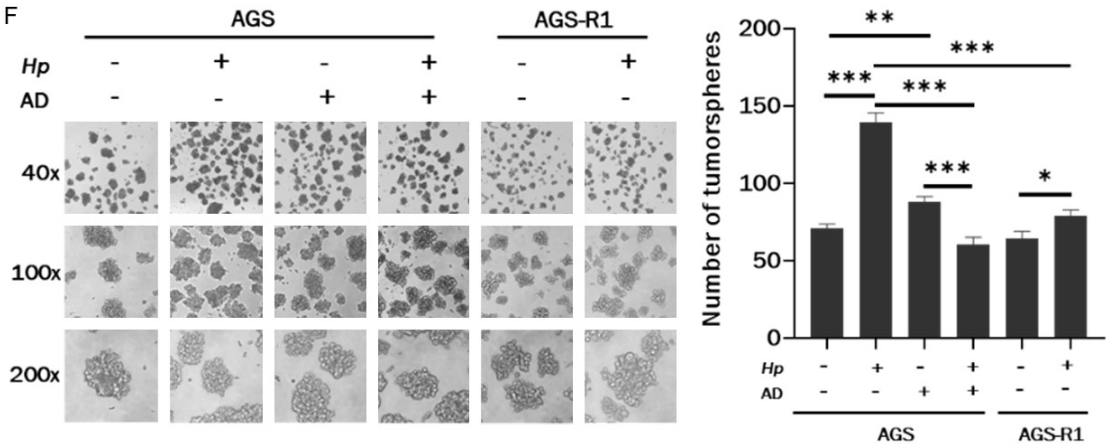

Figure 5. Effect of autophagy on the viability, focus formation, migration, and sphere formation of AGS and AGS-R1 cells with or without *H. pylori* infection. To induce autophagy in AGS cells, AD (5 μM) was added for 3 h, followed by co-culturing with *H. pylori* for another 24 h. To block autophagy, the *Atg5* gene was knocked out by the CRISPR/Cas9 system in AGS cells and co-cultured with *H. pylori* for 24 h. (A) Cell proliferation was determined by MTT assay using a Multiskan™ Sky Microplate Spectrophotometer at 570 nm wavelength. (B) Cytotoxicity was measured by subtracting LDH content in remaining viable cells from total LDH in untreated controls. Error bars represent mean ± SD. Data were analyzed by the Student's t-test. *: $P<0.05$; **: $P<0.01$; ***: $P<0.001$. (C) AGS cells were treated with AD (5 μM) for 3 h, and the medium was replaced with fresh medium containing or not containing *H. pylori* (MOI=150) for another 24 h. To block autophagy, the *Atg5* gene was knocked out by the CRISPR/Cas9 system in AGS cells and co-cultured with *H. pylori* for 24 h. Focus formation was measured at day 7 after treatment. The values shown are the mean ± SD of three independent experiments. (D) After seeding AGS or AGS-R1 (*Atg5* knockout) cells (8×10^5) in a 12-well plate for 24 h, the cells were pretreated with AD (5 μM) for 3 h, followed by evaluation of AGS cell migration with or without *H. pylori* (MOI=75) infection. Representative images of each group at the indicated time points after gap formation are shown. The white dotted lines represent the wound boundary. Quantification is shown in the diagram. (E) Transwell™ migration assay was conducted at 72 h after seeding the cells (5×10^4) under the same conditions as in (A). The quantification of 5 randomly selected fields is shown. The values shown are the mean ± SD of three independent experiments. Data were analyzed using the Student's t-test. *$P<0.05$, **$P<0.01$, ***$P<0.001$. (F) AGS cells (5000 cells/well) were maintained in DMEM/F12 serum-free medium and supplied with 1× B27, bFGF (20 ng/ml), EGF (20 ng/ml), and insulin (5 μg/ml). The suspended cells were maintained in ultra-low attachment 6-well plates. After 7 days, the tumor spheres were formed. The number of tumor spheres was counted when the diameter was greater than 50 μm. *: $P<0.05$; **: $P<0.01$; ***: $P<0.001$.

less of infection status (**Figure 5E**, columns 1 and 2 vs. 5 and 6).

In summary, our findings demonstrated that *H. pylori* infection suppressed cell viability and colony formation, while inducing autophagy activity, migration, and sphere formation in GC cells. When autophagy was further enhanced by an inducer, all *H. pylori*-related malignant features were evidently suppressed. These results indicate that increasing autophagy activity plays a suppressive role in GC tumorigenesis.

Effect of AD-induced autophagy on tumor formation in the xenograft gastric cancer nude mouse model

To validate our *in vitro* findings, we investigated the effects of *H. pylori* infection and enhanced autophagy on tumor formation in a gastric cancer xenograft mouse model. Mice were divided into six groups: (i) AGS; (ii) AGS + *H. pylori*; (iii) AGS + AD (autophagy inducer); (iv) AGS + *H. pylori* + AD; (v) AGS-R1 (*Atg5* KO); and (vi) AGS-R1 + *H. pylori*. A total of 5×10^6 AGS cells, with or without *H. pylori* infection, were subcutaneously injected into nude mice. Three days post-inoculation, mice in the AD-treated groups received intraperitoneal injections of AD (30 mg/kg) every three days for two months.

Initial tumor growth was detected at three weeks post-injection in all groups. The largest tumor volume at this early stage was detected in the mice injected with AGS cells co-cultured with *H. pylori*, followed by AGS + *H. pylori* + AD (**Figure 6A**). At the end of the two-month observation, no detectable tumors remained in either the AGS + *H. pylori* or AGS + *H. pylori* + AD

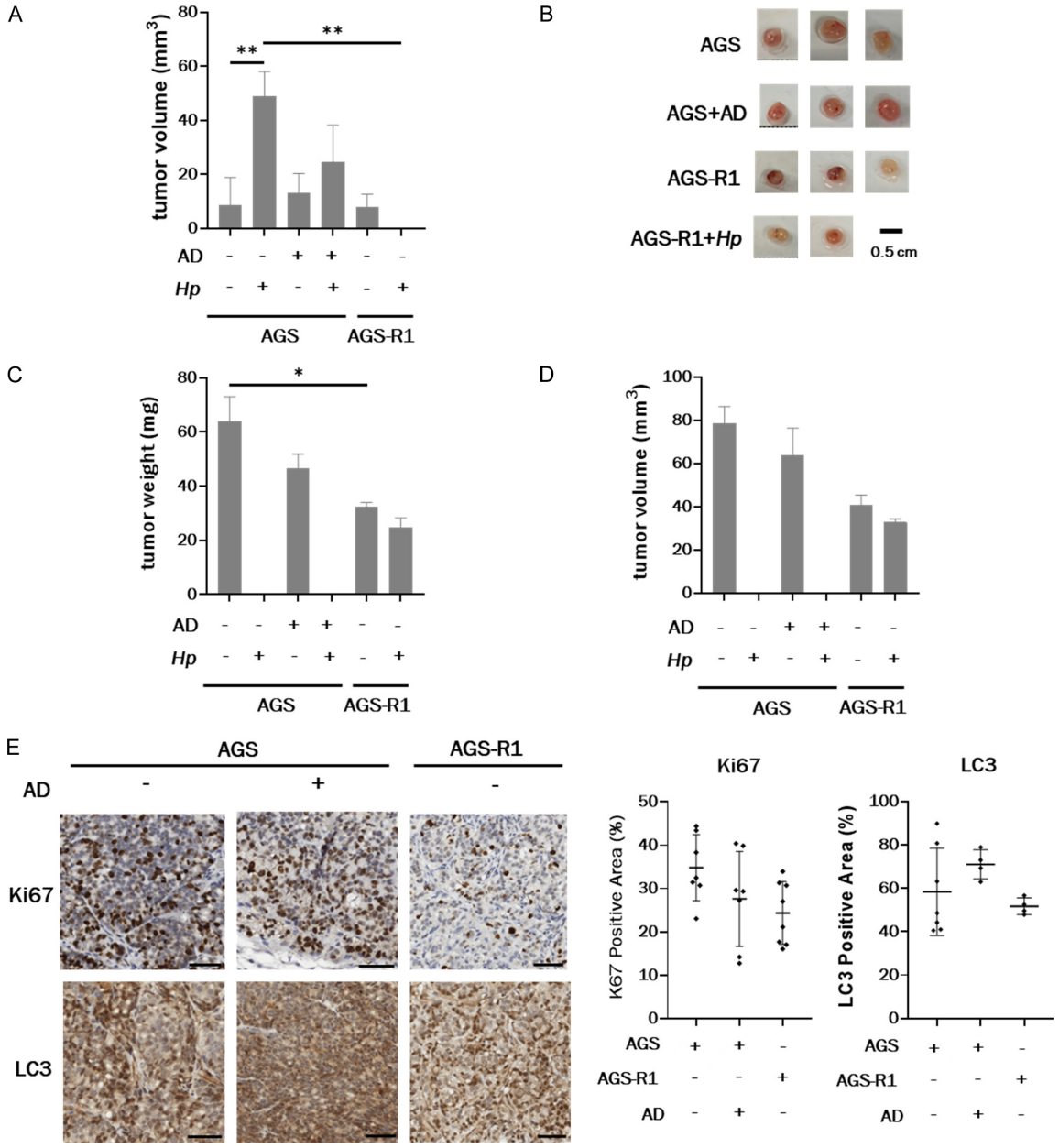

Figure 6. Effect of increased autophagy activity on the tumor formation of wild-type and *Atg5* knockout AGS cells in the xenograft GC nude mouse model. AGS cells (2×10^6 cells in 100 μl of PBS) were inoculated subcutaneously into the 7-week-old nude mice. (A) Tumor size was measured from the surface of the mouse body three weeks after cell injection. Two months later, all the mice were sacrificed, and (B) the photograph of the excised tumors, (C) tumor weight, and (D) volume were measured two months after AGS cell inoculation. Statistical significance between groups was determined with the Student's t-test. **P*<0.05. (E) Representative IHC images showed Ki67 and LC3 protein expression levels in subcutaneous tumor tissues. Scale bar =50 um. Magnification: 20X. Quantitative analysis of the IHC staining intensity using ImageJ software. The values shown are expressed as the mean ± SD. **P*<0.05.

groups (**Figure 6B**), indicating spontaneous tumor regression of AGS cells upon *H. pylori* infection. Among the groups with persistent tumor growth, the AGS group exhibited the highest tumor volume and weight, followed by the AGS + AD group. Notably, the AGS-R1 group showed markedly reduced tumor size compared with the AGS group. However, *H. pylori* suppression of tumor formation in the AGS + *H. pylori* group was counteracted in the

AGS-R1 + *H. pylori* group (**Figure 6C** and **6D**). Immunohistochemical analysis revealed that the proliferation marker Ki67 was expressed at the highest level in the AGS group, followed by the AGS + AD and AGS-R1 groups, consistent with their observed tumorigenicity (**Figure 6E**). The autophagy marker LC3 was expressed most strongly in the AGS + AD group. In contrast, the lowest levels were observed in the AGS-R1 group, consistent with *Atg5* gene knockout.

Taken together, our *in vivo* results indicate that both *H. pylori* infection and enhanced autophagy suppress sustained tumor growth, which is consistent with our *in vitro* findings regarding malignant phenotypes. While *H. pylori* infection may transiently promote early tumor initiation, long-term tumor progression is ultimately restrained.

Discussion

Mitochondrial function plays dual roles during cancer development, including energy metabolism, oxidative stress, and tumorigenesis. Cancer cells rapidly proliferate and commonly reprogram their metabolism from mitochondrial oxidative phosphorylation (OXPHOS) to aerobic glycolysis (Warburg effect) [54]. Moreover, mitochondrial dysfunction also results in oxidative stress through reactive oxygen species (ROS) accumulation, which promotes tumorigenesis through stabilizing HIF-α and inducing DNA damage [54, 55].

Mitochondrial dynamics, especially Drp1-mediated fission, is closely related to cancer cell survival and autophagy. Phosphorylation of Drp1at serine 616 (p-Drp-1) induces the mitochondrial fission, which is an early and critical event of apoptosis [14, 15]. Notably, increased mitochondrial fission promotes autophagy, which supports cancer cell survival depending on the context [15, 17]. Thus, determining the role of p-Drp1-mediated fission is crucial for understanding the balance between cell death and survival.

DDX5 is essential for mitochondrial respiration and growth of Small Cell Lung Cancer (SCLC) [13]. It promotes GC proliferation via the mTOR signaling pathway. Given DDX5's established role in mitochondrial respiration in SCLC, its influence on gastric cancer warrants further investigation. Nonetheless, *H. pylori*-mediated mitochondrial regulation in GC tumorigenesis has rarely been reported.

In this study, we investigated the interplay among *H. pylori* infection, autophagy activity, and mitochondria function in gastric cancer. We reveal three key findings. First, *H. pylori* induces autophagy while simultaneously disrupting mitochondrial fission. Second, autophagy induction suppresses *H. pylori*-induced GC malignancy both *in vitro* and *in vivo*. Third, *H. pylori* activates multiple signaling pathways to regulate GC progression, including the Erk1/2 and JNK MAPK pathways to induce autophagy, while modulating NF-κB and PI3K/Akt-related signaling to influence immune and proliferative responses. These signaling pathways act together to balance survival and death of GC cells (**Figures 7** and S2, S3). In addition, we integrated *in vitro* and i*n vivo* data to clarify the role of autophagy activation in the context of *H. pylori* infection in various GC malignant features. Moreover, G9a mediates H3K9me2, a repressive histone mark, to downregulate autophagy-related genes, including Beclin-1 [51], which supports the postulation that *H. pylori* induces autophagy through G9a-related epigenetic regulation of autophagy-related genes. The abrogation of mitochondrial fission caused by decreased p-Drp1, related to mitophagy, an important mediator of mitochondrial quality control in cardiomyocytes, has been reported [56].

Our mitochondria activity and ROS data suggest that *H. pylori* infection pushes the GC cells' mitochondria to work harder, possibly in an attempt to meet an increased energy demand or to compensate for some other cellular stress induced by the infection. However, this overdrive is inefficient or dysregulated, leading to an increase in harmful reactive oxygen species. This can be interpreted as a form of mitochondrial dysfunction or stress response, where the increased metabolic output is coupled with heightened oxidative damage (**Figure 2E** and **2F**). This speculation is consistent with what is known about *H. pylori* infection, which is often associated with oxidative stress and mitochondrial dysfunction in gastric cells, contributing to gastric inflammation and potentially cancer development [53].

While *H. pylori* infection simultaneously triggers pro-tumorigenic features (transient tumor for-

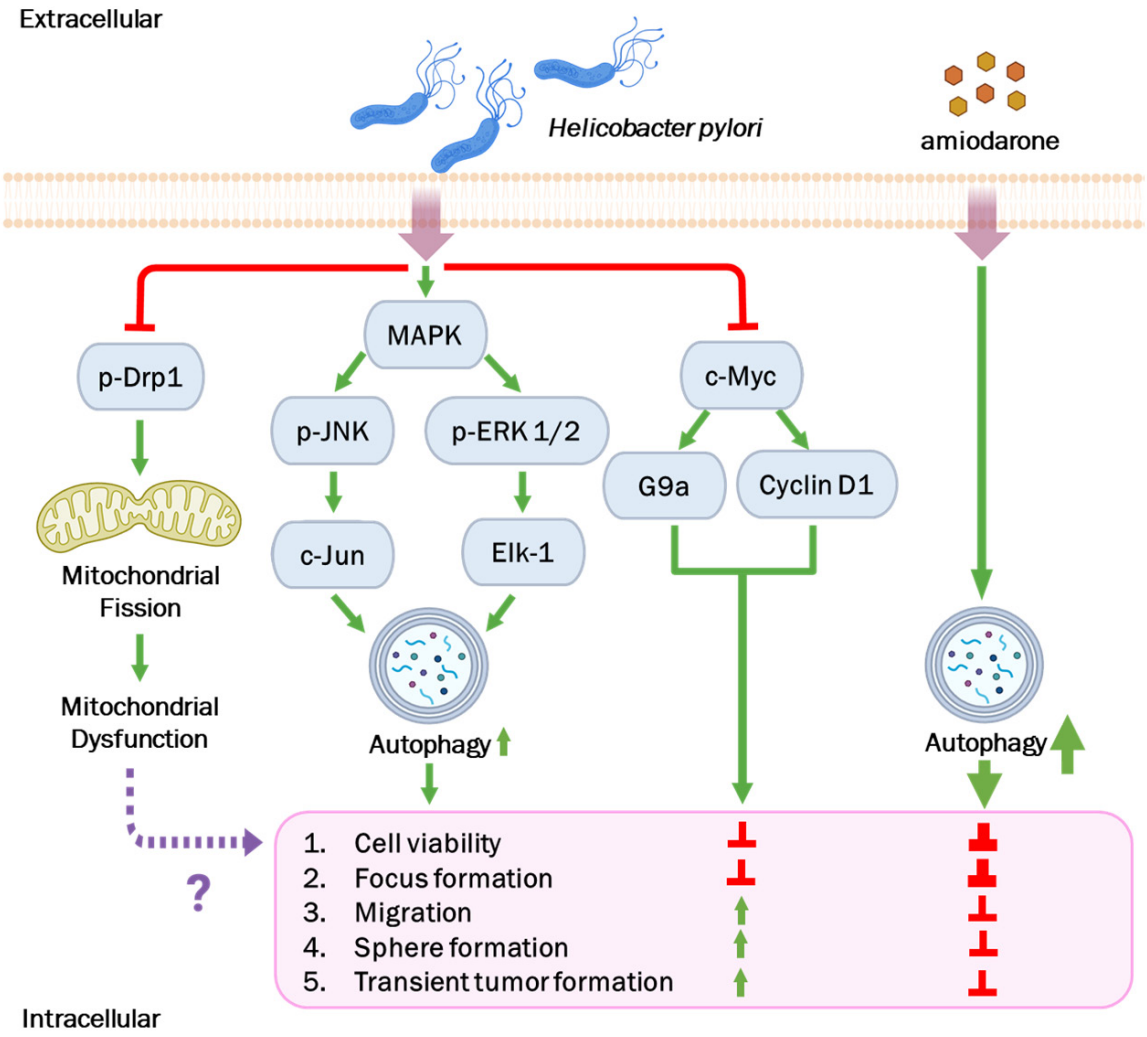

Figure 7. Proposed schematic model illustrating the role of *H. pylori* infection in regulating autophagy and gastric cancer malignant features. *H. pylori* infection activates MAPK/ERK and JNK signaling pathways, which in turn promote autophagy. Treatment with the autophagy inducer amiodarone further enhances autophagic activity and is associated with reduced gastric cancer-associated malignant phenotypes, including cell viability, focus formation, migration, sphere formation, and tumor growth. Directional arrows indicate the regulatory relationships between signaling components, and labels highlight key pathway interactions described in this study. Some of the images were created at https://BioRender.com.

mation, migration and sphere formation) and autophagy activation, the infection-induced autophagy alone appears insufficient to restrain tumor progression. This observation suggests that *H. pylori*-driven tumorigenesis also involves autophagy-independent mechanisms, including chronic inflammation, ROS-induced DNA damage, and dysregulation of host signaling pathways [24, 57]. In contrast, pharmacological enhancement of autophagy led to pronounced tumor-suppressive effects, underscoring autophagy as a protective mechanism that can counteract *H. pylori*-induced oncogenic signaling.

While increased LC3-II accumulation and autophagy-related vesicle formation were observed following *H. pylori* infection, these findings do not fully distinguish between enhanced autophagic flux and impaired autophagosome degradation. Our preliminary data showed that *H. pylori* infection in GC cells resulted in a temporal increase in LC3-II levels from 0 to 24 h; however, no subsequent LC3-II degradation was observed, suggesting a potential impairment in autophagy progression. In contrast, chloroquine-mediated fusion blockade experiments indicated that H. pylori induces partial autophagic flux (**Figure 3A**, lane 3 vs. 7; **Figure**

3B, lane 2 vs. 6). Together, these observations underscore the need for further investigation to more precisely characterize autophagic flux in the context of *H. pylori* infection. Moreover, our mitochondrial respiration and ROS analyses suggest that *H. pylori*-induced metabolic stress leads to elevated oxidative stress, which may promote DNA damage and genomic instability. Enhanced autophagy may counteract these effects by facilitating mitochondrial quality control and limiting excessive ROS accumulation, thereby contributing to tumor-suppressive outcomes.

The increased expression of LC3 and p-Drp1 in patient tumor tissues implies the importance of the abnormal autophagy activity and mitochondrial dynamics in GC. Furthermore, our observation that *H. pylori* infection increases autophagy activity and suppresses GC cell tumorigenesis supports the findings of Courtois *et al.*, who reported increased autophagy through mTORC1 inhibition and ULK1 upregulation in response to *H. pylori* infection [58]. Our previous studies showed that autophagosomes selectively degrade oncogenic molecules, including miR-224 and cyclin D1 in liver cancer cells to suppress tumorigenesis [59], which parallels the downregulation of cyclin D1 observed in *H. pylori*-infected GC cells, accompanied by the increased autophagy activity (**Figure 3A** and **3B**).

We have reported that 1) Ha-*ras*^{val12}-related tumorigenesis is suppressed by an Erk1/2-BNIP3-mediated autophagy activation [60]; 2) DENV infection-induced IRE1α-JNK signaling pathway increases autophagy activity through phosphorylation of JNK and downstream molecule Bcl-2, which then dissociates from Beclin 1 to result in autophagy activation [61]. These findings support a model in which *H. pylori*-mediated activation of the Erk1/2 and JNK pathways promotes autophagy induction, whereas enhanced autophagy does not exert reciprocal effects on ELK1 or c-Jun activity (**Figures 7** and S3).

In addition, our RNA-seq and protein analyses demonstrate the involvement of multiple signaling pathways previously implicated in *H. pylori*-related GC, including the MAPK, PI3K-Akt-mTOR, Wnt/β-catenin, and JAK-STAT pathways [22].

H. pylori has been classified as a Group 1 carcinogen by the WHO since 1994, and chronic infection increases the risk of gastric cancer [62]. It has been reported that *H. pylori* infection induces chronic gastritis, DNA damage through reactive oxygen species, and dysregulation of host signaling pathways, all of which contribute to gastric carcinogenesis [63]. Although *H. pylori* infection transiently promoted tumor formation and enhanced migration and stemness, it concurrently suppressed oncogenic drivers such as G9a, c-Myc, and cyclin D1, ultimately resulting in reduced cell viability *in vitro* and tumor regression *in vivo*. This discrepancy may be due to a stage-dependent process in which early infection promotes malignant traits through inflammation, ROS-mediated DNA damage, and host signaling dysregulation [57], whereas prolonged infection activates stress responses such as autophagy and apoptosis that counteract tumor progression. Thus, the tumorigenic potential of *H. pylori* likely arises from a dynamic balance between transient pro-tumorigenic effects and long-term tumor-suppressive mechanisms, highlighting the need to delineate the spatial and temporal contributions of the tumor microenvironment during *H. pylori* infection.

Previous studies have reported that *H. pylori*-induced autophagy can be subverted by the bacterium to facilitate intracellular survival rather than tumor suppression [22]. In contrast, when autophagy was further pharmacologically enhanced beyond basal levels, we observed robust suppression of *H. pylori*-related malignant traits, suggesting that sufficiently elevated autophagy activity exerts a tumor-suppressive effect.

This study integrates *in vitro* and *in vivo* data to clarify the autophagic response to *H. pylori* infection in gastric cancer. However, our study has several limitations. One limitation of the present *in vivo* study is the use of immunodeficient nude mice, which lack functional T lymphocytes. While this model is well suited for evaluating tumor-intrinsic effects of autophagy modulation on gastric cancer growth, it does not fully capture the contribution of adaptive immunity or tumor-immune microenvironment interactions. Autophagy has been shown to influence antigen presentation, immune cell recruitment, and inflammatory signaling, all of

which may critically shape tumor progression in the context of *H. pylori* infection [22, 64]. Therefore, future studies employing immunocompetent mouse models, such as *H. pylori*-infected C57BL/6 mice or syngeneic gastric cancer models, will be essential to clarify how autophagy regulates immune surveillance, immune evasion, and tumor-host interactions during gastric carcinogenesis. Another limitation is the lack of temporal and stage-specific analyses of autophagy during different phases of *H. pylori* infection and gastric cancer progression. Autophagy is a highly dynamic process that may exert distinct effects during early infection, chronic inflammation, tumor initiation, and advanced malignancy *in vivo*. Our findings therefore represent a specific time point of autophagy regulation rather than a longitudinal assessment. Future studies incorporating time-course analyses and stratification by tumor grade or infection duration will be critical to fully elucidate the context-dependent roles of autophagy in gastric carcinogenesis.

Although we demonstrated a tumor-suppressive effect by increasing autophagy activity, the underlying mechanisms - specifically whether tumor suppression is mediated through apoptosis or reduced DNA replication - remain to be clarified. Moreover, although our data suggest the role of autophagy in modulating immune pathways such as NF-κB and STAT3 pathways, these were not functionally validated in immunocompetent models. Additionally, although patient tissue analyses showed higher autophagy LC3 and mitochondria marker p-Drp1 expression in tumors, their predictive or prognostic value was not evaluated through survival analysis. Although increased LC3 and p-Drp1 expression were consistently observed in gastric cancer tissues, exploratory Kaplan-Meier survival analyses did not demonstrate statistically significant differences, likely due to limited long-term follow-up data and insufficient statistical power of the patient cohort; therefore, these results were not presented in the Results section. Nevertheless, accumulating evidence suggests that dysregulated autophagy and mitochondrial dynamics are closely associated with patient prognosis in multiple solid tumors, including gastric cancer. Elevated autophagy activity has been linked to tumor adaptation to metabolic stress, while altered Drp1-mediated mitochondrial fission has been implicated in tumor aggressiveness and therapy resistance [65-67]. Our findings support the clinical relevance of LC3 and p-Drp1 as potential biomarkers reflecting metabolic and stress-adaptive states in *H. pylori*-associated gastric cancer. Future large-scale studies integrating survival data will be necessary to determine their prognostic value and therapeutic utility.

Amiodarone, a clinically approved anti-arrhythmic agent, was employed in this study as a pharmacological tool to further interrogate the functional role of autophagy in *H. pylori*-associated gastric cancer [68]. Importantly, amiodarone was used as a proof-of-concept autophagy modulator rather than as an immediately translatable anticancer drug. Its established clinical use and well-characterized pharmacological profile provide a framework for considering drug repurposing strategies targeting autophagy-related pathways [69]. Nevertheless, the clinical applicability of amiodarone in oncology is constrained by its known dose-dependent toxicities, including pulmonary, hepatic, and thyroid adverse effects [70, 71]. These safety concerns underscore the necessity for careful dose optimization, treatment scheduling, and patient selection in any future oncological application. Therefore, the findings of the present study should be interpreted as mechanistic evidence supporting autophagy modulation, rather than direct clinical endorsement of amiodarone as a therapeutic agent. In addition, autophagy has been implicated in modulating responses to both chemotherapy and immunotherapy [21, 72]. Pharmacological modulation of autophagy may enhance chemosensitivity or influence tumor immune responses, suggesting that amiodarone or related autophagy-targeting strategies could potentially be explored in combination with standard gastric cancer therapies. However, such combination approaches remain speculative and will require comprehensive preclinical and clinical evaluation to assess efficacy and safety.

In conclusion, our findings provide compelling evidence that *H. pylori* infection induces autophagy and impairs mitochondrial function in gastric cancer cells. Enhanced autophagy activity suppresses malignant transformation both *in vitro* and *in vivo*. The *H. pylori*-mediated downregulation of c-Myc, G9a, and cyclin D1, together with activation of signaling pathways

such as p-Erk1/2 and p-JNK, promotes autophagy and collectively suggests that autophagy exerts broad regulatory effects in *H. pylori*-associated gastric cancer tumorigenesis. Future studies will focus on genome-wide epigenetic profiling of G9a and the preclinical and clinical evaluation of autophagy inducer-based combination therapies to further validate our findings and facilitate their translation into precision medicine strategies.

Acknowledgements

We thank the Center for Laboratory Animals in Kaohsiung Medical University for the animal care; the Center for Research Resources and Development in Kaohsiung Medical University for their assistance with TissueFAXS and confocal image analysis. We also thank the Ultrastructural Laboratory, Division of Research Resource, Department of Medical Research, Kaohsiung Medical University Hospital for providing technical assistance. This research was funded by Kaohsiung Medical University Research Center Grant (grant number: KMU-TC114A04), National Science and Technology Council, Taiwan (grant number: MOST 109-2314-B-037-120-, MOST 110-2314-B-037-142-, MOST 111-2314-B-037-010-, NSTC 114-2314-B-037-103-MY3, NSTC 114-2321-B-037-003, and NSTC 113-2314-B-037-059-MY3), and Kaohsiung Medical University Hospital Grant (KMUH109-9R03 and KMUH113-3R31).

Disclosure of conflict of interest

The authors declare that the research was conducted in the absence of any commercial or financial relationships that could be construed as a potential conflict of interest.

Address correspondence to: Deng-Chyang Wu, Division of Gastroenterology, Department of Internal Medicine, Kaohsiung Medical University Hospital, Kaohsiung 807378, Taiwan. E-mail: dechwu@kmu.edu.tw; Hsiao-Sheng Liu, Tropical Medicine, Kaohsiung Medical University, Kaohsiung 807378, Taiwan. E-mail: hsliu713@kmu.edu.tw

References

[1] Levine B and Kroemer G. Autophagy in the pathogenesis of disease. Cell 2008; 132: 27-42.

[2] Marshall BJ and Warren JR. Unidentified curved bacilli in the stomach of patients with gastritis and peptic ulceration. Lancet 1984; 1: 1311-1315.

[3] Lee BM, Jang JJ, Kim JS, You YC, Chun SA, Kim HS, Han HM, Ahn MY and Byun SH. Association of Helicobacter pylori infection with gastric adenocarcinoma. Jpn J Cancer Res 1998; 89: 597-603.

[4] Chophel T, Tshering S, Dorji N and Tshomo U. Stomach cancer screening services of bhutan. Indian J Surg 2022; 1-6.

[5] Leclerc H. Epidemiological aspects of Helicobacter pylori infection. Bull Acad Natl Med 2006; 190: 949-962.

[6] Greenfield LK and Jones NL. Modulation of autophagy by Helicobacter pylori and its role in gastric carcinogenesis. Trends Microbiol 2013; 21: 602-612.

[7] Li N, Tang B, Jia YP, Zhu P, Zhuang Y, Fang Y, Li Q, Wang K, Zhang WJ, Guo G, Wang TJ, Feng YJ, Qiao B, Mao XH and Zou QM. Helicobacter pylori CagA protein negatively regulates autophagy and promotes inflammatory response via c-Met-PI3K/Akt-mTOR signaling pathway. Front Cell Infect Microbiol 2017; 7: 417.

[8] Tong T, Zhou Y, Huang Q, Xiao C, Bai Q, Deng B and Chen L. The regulation roles of miRNAs in Helicobacter pylori infection. Clin Transl Oncol 2023; 25: 1929-1939.

[9] Song Y, Liu P, Qi X, Shi XL, Wang YS, Guo D, Luo H, Du ZJ and Wang MY. Helicobacter pylori infection delays neutrophil apoptosis and exacerbates inflammatory response. Future Microbiol 2024; 19: 1145-1156.

[10] Levine B and Kroemer G. Biological functions of autophagy genes: a disease perspective. Cell 2019; 176: 11-42.

[11] Kabeya Y, Mizushima N, Ueno T, Yamamoto A, Kirisako T, Noda T, Kominami E, Ohsumi Y and Yoshimori T. LC3, a mammalian homologue of yeast Apg8p, is localized in autophagosome membranes after processing. EMBO J 2000; 19: 5720-5728.

[12] Debnath J, Gammoh N and Ryan KM. Autophagy and autophagy-related pathways in cancer. Nat Rev Mol Cell Biol 2023; 24: 560-575.

[13] Das S, Zea MP, Russon MP, Xing Z, Torregrosa-Allen S, Cervantes HE, Harper HA, Elzey BD and Tran EJ. Supinoxin blocks small cell lung cancer progression by inhibiting mitochondrial respiration through DDX5. iScience 2025; 28: 112219.

[14] Thomas KJ and Jacobson MR. Defects in mitochondrial fission protein dynamin-related protein 1 are linked to apoptotic resistance and autophagy in a lung cancer model. PLoS One 2012; 7: e45319.

[15] Deng X, Liu J, Liu L, Sun X, Huang J and Dong J. Drp1-mediated mitochondrial fission contributes to baicalein-induced apoptosis and autophagy in lung cancer via activation of AMPK signaling pathway. Int J Biol Sci 2020; 16: 1403-1416.
[16] Bordi M, Nazio F and Campello S. The close interconnection between mitochondrial dynamics and mitophagy in cancer. Front Oncol 2017; 7: 81.
[17] Huang Q, Zhan L, Cao H, Li J, Lyu Y, Guo X, Zhang J, Ji L, Ren T, An J, Liu B, Nie Y and Xing J. Increased mitochondrial fission promotes autophagy and hepatocellular carcinoma cell survival through the ROS-modulated coordinated regulation of the NFKB and TP53 pathways. Autophagy 2016; 12: 999-1014.
[18] Javed Z, Shin DH, Pan W, White SR, Elhaw AT, Kim YS, Kamlapurkar S, Cheng YY, Benson JC, Abdelnaby AE, Phaëton R, Wang HG, Yang S, Sullivan MLG, St Croix CM, Watkins SC, Mullett SJ, Gelhaus SL, Lee N, Coffman LG, Aird KM, Trebak M, Mythreye K, Walter V and Hempel N. Drp1 splice variants regulate ovarian cancer mitochondrial dynamics and tumor progression. EMBO Rep 2024; 25: 4281-4310.
[19] Shibata T, Imoto I and Gabazza EC. Detection of Helicobacter pylori in biopsy of patients with gastric carcinoma. Biomed Pharmacother 1997; 51: 22-28.
[20] He Y, Wang C, Zhang X, Lu X, Xing J, Lv J, Guo M, Huo X, Liu X, Lu J, Du X, Li C and Chen Z. Sustained exposure to helicobacter pylori lysate inhibits apoptosis and autophagy of gastric epithelial cells. Front Oncol 2020; 10: 581364.
[21] Xu JL, Yuan L, Tang YC, Xu ZY, Xu HD, Cheng XD and Qin JJ. The role of autophagy in gastric cancer chemoresistance: friend or foe? Front Cell Dev Biol 2020; 8: 621428.
[22] Yang Y, Shu X and Xie C. An overview of autophagy in helicobacter pylori infection and related gastric cancer. Front Cell Infect Microbiol 2022; 12: 847716.
[23] Watanabe T, Asano N, Kudo M and Strober W. Nucleotide-binding oligomerization domain 1 and gastrointestinal disorders. Proc Jpn Acad Ser B Phys Biol Sci 2017; 93: 578-599.
[24] Zhang F, Chen C, Hu J, Su R, Zhang J, Han Z, Chen H and Li Y. Molecular mechanism of Helicobacter pylori-induced autophagy in gastric cancer. Oncol Lett 2019; 18: 6221-6227.
[25] Lai CH, Huang JC, Cheng HH, Wu MC, Huang MZ, Hsu HY, Chen YA, Hsu CY, Pan YJ, Chu YT, Chen TJ, Wu YF, Sit WY, Liu JS, Chiu YF, Wang HJ and Wang WC. Helicobacter pylori cholesterol glucosylation modulates autophagy for increasing intracellular survival in macrophages. Cell Microbiol 2018; 20: e12947.
[26] Qin W, Li C, Zheng W, Guo Q, Zhang Y, Kang M, Zhang B, Yang B, Li B, Yang H and Wu Y. Inhibition of autophagy promotes metastasis and glycolysis by inducing ROS in gastric cancer cells. Oncotarget 2015; 6: 39839-39854.
[27] Xin L, Zhou Q, Yuan YW, Zhou LQ, Liu L, Li SH and Liu C. METase/lncRNA HULC/FoxM1 reduced cisplatin resistance in gastric cancer by suppressing autophagy. J Cancer Res Clin Oncol 2019; 145: 2507-2517.
[28] Nie H, Wang Y, Qin Y and Gong XG. Oleanolic acid induces autophagic death in human gastric cancer cells in vitro and in vivo. Cell Biol Int 2016; 40: 770-778.
[29] Yuan Y, He X, Li X, Liu Y, Tang Y, Deng H and Shi X. Narciclasine induces autophagy-mediated apoptosis in gastric cancer cells through the Akt/mTOR signaling pathway. BMC Pharmacol Toxicol 2021; 22: 70.
[30] Li JP, Zhang HM, Liu MJ, Xiang Y, Li H, Huang F, Li HH, Dai ZT, Gu CJ, Liao XH and Zhang TC. miR-133a-3p/FOXP3 axis regulates cell proliferation and autophagy in gastric cancer. J Cell Biochem 2020; 121: 3392-3405.
[31] Xue Y, Wang J, He Y, Patra P and Gao YQ. Multiscale gene regulation mechanism: spatiotemporal transmission of genetic information. Curr Opin Struct Biol 2022; 77: 102487.
[32] Dawson MA and Kouzarides T. Cancer epigenetics: from mechanism to therapy. Cell 2012; 150: 12-27.
[33] Prabhakaran R, Thamarai R, Sivasamy S, Dhandayuthapani S, Batra J, Kamaraj C, Karthik K, Shah MA and Mallik S. Epigenetic frontiers: miRNAs, long non-coding RNAs and nanomaterials are pioneering to cancer therapy. Epigenetics Chromatin 2024; 17: 31.
[34] Labbé C, Robles V and Herraez MP. Epigenetics in fish gametes and early embryo. Aquaculture 2017; 472: 93-106.
[35] Kishore C. Epigenetic regulation and promising therapies in colorectal cancer. Curr Mol Pharmacol 2021; 14: 838-852.
[36] Correction: UTX and MLL4 coordinately regulate transcriptional programs for cell proliferation and invasiveness in breast cancer cells. Cancer Res 2017; 77: 2553.
[37] Komatsu K, Ideno H, Nakashima K, Udagawa N, Kobayashi Y, Kimura H, Tachibana M, Yamashita T and Nifuji A. The G9a histone methyltransferase represses osteoclastogenesis and bone resorption by regulating NFATc1 function. FASEB J 2024; 38: e23779.
[38] Park KE, Johnson CM and Cabot RA. IVM-BIX-01294, an inhibitor of the histone methyltransferase EHMT2, disrupts histone H3 lysine 9 (H3K9) dimethylation in the cleavage-stage porcine embryo. Reprod Fertil Dev 2012; 24: 813-821.

[39] Lu Z, Tian Y, Salwen HR, Chlenski A, Godley LA, Raj JU and Yang Q. Histone-lysine methyltransferase EHMT2 is involved in proliferation, apoptosis, cell invasion, and DNA methylation of human neuroblastoma cells. Anticancer Drugs 2013; 24: 484-493.

[40] Urrutia G, de Assuncao TM, Mathison AJ, Salmonson A, Kerketta R, Zeighami A, Stodola TJ, Adsay V, Pehlivanoglu B, Dwinell MB, Zimmermann MT, Iovanna JL, Urrutia R and Lomberk G. Inactivation of the euchromatic histone-lysine N-methyltransferase 2 pathway in pancreatic epithelial cells antagonizes cancer initiation and pancreatitis-associated promotion by altering growth and immune gene expression networks. Front Cell Dev Biol 2021; 9: 681153.

[41] Yu YS, Kim H, Kim KI and Baek SH. Epigenetic regulation of autophagy by histone-modifying enzymes under nutrient stress. Cell Death Differ 2023; 30: 1430-1436.

[42] Park SE, Yi HJ, Suh N, Park YY, Koh JY, Jeong SY, Cho DH, Kim CS and Hwang JJ. Correction: inhibition of EHMT2/G9a epigenetically increases the transcription of Beclin-1 via an increase in ROS and activation of NF-κB. Oncotarget 2019; 10: 4348-4349.

[43] Hashemi M, Mohandesi Khosroshahi E, Tanha M, Khoushab S, Bizhanpour A, Azizi F, Mohammadzadeh M, Matinahmadi A, Khazaei Koohpar Z, Asadi S, Taheri H, Khorrami R, Ramezani Farani M, Rashidi M, Rezaei M, Fattah E, Taheriazam A and Entezari M. Targeting autophagy can synergize the efficacy of immune checkpoint inhibitors against therapeutic resistance: new promising strategy to reinvigorate cancer therapy. Heliyon 2024; 10: e37376.

[44] Wang H, Sun P, Yuan X, Xu Z, Jiang X, Xiao M, Yao X and Shi Y. Autophagy in tumor immune escape and immunotherapy. Mol Cancer 2025; 24: 85.

[45] Michetti F, Cirone M, Strippoli R, D'Orazi G and Cordani M. Mechanistic insights and therapeutic strategies for targeting autophagy in pancreatic ductal adenocarcinoma. Discov Oncol 2025; 16: 592.

[46] Halder P, Datta C, Kumar R, Sharma AK, Basu J and Kundu M. The secreted antigen, HP0175, of Helicobacter pylori links the unfolded protein response (UPR) to autophagy in gastric epithelial cells. Cell Microbiol 2015; 17: 714-729.

[47] Li FY, Weng IC, Lin CH, Kao MC, Wu MS, Chen HY and Liu FT. Helicobacter pylori induces intracellular galectin-8 aggregation around damaged lysosomes within gastric epithelial cells in a host O-glycan-dependent manner. Glycobiology 2019; 29: 151-162.

[48] Akbari A, Noorbakhsh Varnosfaderani SM, Haeri MS, Fathi Z, Aziziyan F, Yousefi Rad A, Zalpoor H, Nabi-Afjadi M and Malekzadegan Y. Autophagy induced by Helicobacter Pylori infection can lead to gastric cancer dormancy, metastasis, and recurrence: new insights. Hum Cell 2024; 37: 139-153.

[49] Schläfli AM, Berezowska S, Adams O, Langer R and Tschan MP. Reliable LC3 and p62 autophagy marker detection in formalin fixed paraffin embedded human tissue by immunohistochemistry. Eur J Histochem 2015; 59: 2481.

[50] Lima AR, Correia M, Santos L, Tavares C, Rios E, Canberk S, Soares P, Sobrinho-Simões M, Melo M and Máximo V. S616-p-DRP1 associates with locally invasive behavior of follicular cell-derived thyroid carcinoma. Endocrine 2021; 73: 85-97.

[51] Cao YP, Sun JY, Li MQ, Dong Y, Zhang YH, Yan J, Huang RM and Yan X. Inhibition of G9a by a small molecule inhibitor, UNC0642, induces apoptosis of human bladder cancer cells. Acta Pharmacol Sin 2019; 40: 1076-1084.

[52] Bellamy J, Szemes M, Melegh Z, Dallosso A, Kollareddy M, Catchpoole D and Malik K. Increased efficacy of histone methyltransferase G9a inhibitors against MYCN-amplified neuroblastoma. Front Oncol 2020; 10: 818.

[53] Gülow K, Tümen D, Heumann P, Schmid S, Kandulski A, Müller M and Kunst C. Unraveling the role of reactive oxygen species in T lymphocyte signaling. Int J Mol Sci 2024; 25: 6114.

[54] Bao X, Zhang J, Huang G, Yan J, Xu C, Dou Z, Sun C and Zhang H. The crosstalk between HIFs and mitochondrial dysfunctions in cancer development. Cell Death Dis 2021; 12: 215.

[55] Boland ML, Chourasia AH and Macleod KF. Mitochondrial dysfunction in cancer. Front Oncol 2013; 3: 292.

[56] Shirakabe A, Zhai P, Ikeda Y, Saito T, Maejima Y, Hsu CP, Nomura M, Egashira K, Levine B and Sadoshima J. Drp1-dependent mitochondrial autophagy plays a protective role against pressure overload-induced mitochondrial dysfunction and heart failure. Circulation 2016; 133: 1249-1263.

[57] Duan Y, Xu Y, Dou Y and Xu D. Helicobacter pylori and gastric cancer: mechanisms and new perspectives. J Hematol Oncol 2025; 18: 10.

[58] Courtois S, Haykal M, Bodineau C, Sifré E, Azzi-Martin L, Ménard A, Mégraud F, Lehours P, Durán RV, Varon C and Bessède E. Autophagy induced by Helicobacter pylori infection is necessary for gastric cancer stem cell emergence. Gastric Cancer 2021; 24: 133-144.

[59] Wu SY, Lan SH and Liu HS. Degradative autophagy selectively regulates CCND1 (cyclin D1) and MIR224, two oncogenic factors involved in hepatocellular carcinoma tumorigenesis. Autophagy 2019; 15: 729-730.

[60] Wu SY, Lan SH, Cheng DE, Chen WK, Shen CH, Lee YR, Zuchini R and Liu HS. Ras-related tumorigenesis is suppressed by BNIP3-mediated autophagy through inhibition of cell proliferation. Neoplasia 2011; 13: 1171-1182.
[61] Lee YR, Kuo SH, Lin CY, Fu PJ, Lin YS, Yeh TM and Liu HS. Dengue virus-induced ER stress is required for autophagy activation, viral replication, and pathogenesis both in vitro and in vivo. Sci Rep 2018; 8: 489.
[62] Loosen SH, Mertens A, Klein I, Leyh C, Krieg S, Kandler J, Luedde T, Roderburg C and Kostev K. Association between Helicobacter pylori and its eradication and the development of cancer. BMJ Open Gastroenterol 2024; 11: e001377.
[63] Raza Y, Mubarak M, Memon MY and Alsulaimi MS. Update on molecular pathogenesis of Helicobacter pylori-induced gastric cancer. World J Gastrointest Pathophysiol 2025; 16: 107052.
[64] Chen D, Wu L, Liu X, Wang Q, Gui S, Bao L, Wang Z, He X, Zhao Y, Zhou J and Xie Y. Helicobacter pylori CagA mediated mitophagy to attenuate the NLRP3 inflammasome activation and enhance the survival of infected cells. Sci Rep 2024; 14: 21648.
[65] Han R, Wei J, Zhao B and Zhao R. Mitochondrial autophagy-related lncRNAs as prognostic biomarkers and therapeutic targets in gastric adenocarcinoma. Discov Oncol 2025; 16: 283.
[66] Wen W, Ertas YN, Erdem A and Zhang Y. Dysregulation of autophagy in gastric carcinoma: pathways to tumor progression and resistance to therapy. Cancer Lett 2024; 591: 216857.
[67] Gorbunova AS, Zamaraev AV, Yapryntseva MA, Kovaleva OV, Tchevkina EM, Turkina MV, Zhivotovsky B and Kopeina GS. Prognostic signature based on mitochondria quality control proteins for the prediction of lung adenocarcinoma patients survival. Cell Death Discov 2023; 9: 352.
[68] Balgi AD, Fonseca BD, Donohue E, Tsang TC, Lajoie P, Proud CG, Nabi IR and Roberge M. Screen for chemical modulators of autophagy reveals novel therapeutic inhibitors of mTORC1 signaling. PLoS One 2009; 4: e7124.
[69] Lee KY, Oh S, Choi YJ, Oh SH, Yang YS, Yang MJ, Lee K and Lee BH. Activation of autophagy rescues amiodarone-induced apoptosis of lung epithelial cells and pulmonary toxicity in rats. Toxicol Sci 2013; 136: 193-204.
[70] Steinberg E, Fluksman A, Zemmour C, Tischenko K, Karsch-Bluman A, Brill-Karniely Y, Birsner AE, D'Amato RJ and Benny O. Low dose amiodarone reduces tumor growth and angiogenesis. Sci Rep 2020; 10: 18034.
[71] Tsaban G, Ostrovsky D, Alnsasra H, Burrack N, Gordon M, Babayev AS, Omari Y, Kezerle L, Shamia D, Bereza S, Konstantino Y and Haim M. Amiodarone and pulmonary toxicity in atrial fibrillation: a nationwide Israeli study. Eur Heart J 2024; 45: 379-388.
[72] Lei Y, Zhang E, Bai L and Li Y. Autophagy in cancer immunotherapy. Cells 2022; 11: 2996.

Supplementary material and method

RNA sequencing (RNA-Seq) and data analysis

Total RNAs were isolated from AGS cells and *Hp* 49503-infected AGS cells. RNA extraction and sequencing services were provided by Phalanx Biotech Group, Hsinchu, Taiwan.

Illumina TruSeq Stranded mRNA sequencing was performed by Phalanx Biotech following the standard Illumina kit protocol (Illumina, San Diego, CA). Briefly, polyA mRNA from an input of 500 ng high-quality total RNA (RIN value >8) was purified, fragmented, and first- and second-strand cDNA synthesized. Barcoded linkers were ligated to generate indexed libraries. The libraries were quantified using the Promega QuantiFluor dsDNA System on a Quantus Fluorometer (Promega, Madison, WI). The size and purity of the libraries were analyzed using the High Sensitivity D1000 Screen Tape on an Agilent 2100 TapeStation instrument. The libraries were pooled and run on an Illumina sequencer using paired-end 150 bp Rapid Run format to generate 20 million reads per sample. After the reads were aligned to the genome (Ensembl Homo sapiens. GRCh38.104), Cufflinks was used on the resulting alignment files to generate a transcriptome assembly for each condition. Cufflink, a part of the Cuffdiffs package, took the aligned reads and merged assemblies from two or more conditions to estimate the expression levels by calculating the number of RNA-Seq Fragments Per Kilobase of transcript per total Million (FPKM) fragments methods mapped. Cuffdiff tests the statistical significance of observed changes and identifies differentially regulated genes at the transcriptional or post-transcriptional level. The number of differentially expressed genes for each comparison is calculated based on the experimental design. Standard selection criteria to identify differentially expressed genes are as follows: Log_2 fold change (FC) ≥1 or ≤-1 and *p*-value <0.05. KEGG pathways enrichment analysis was performed using the differentially expressed gene lists as input.

Table S1. The number of GC patients and the definition of GC patient parameters

Parameters	Definition	Number
Gender		
	Male	100
	Female	60
Age (year)		
	Range	24-91
	Mean	64.4
	<64	81
	≥64	79
TNM stage		
	Stage 1-2	74
	Stage 3-4	86
Tumor size		
	Range	1.5-999
	Median	48
	<48	86
	≥48	74
Lymphatic or vascular invasion		
	Yes	87
	No	73
Nerve invasion		
	Yes	94
	No	66

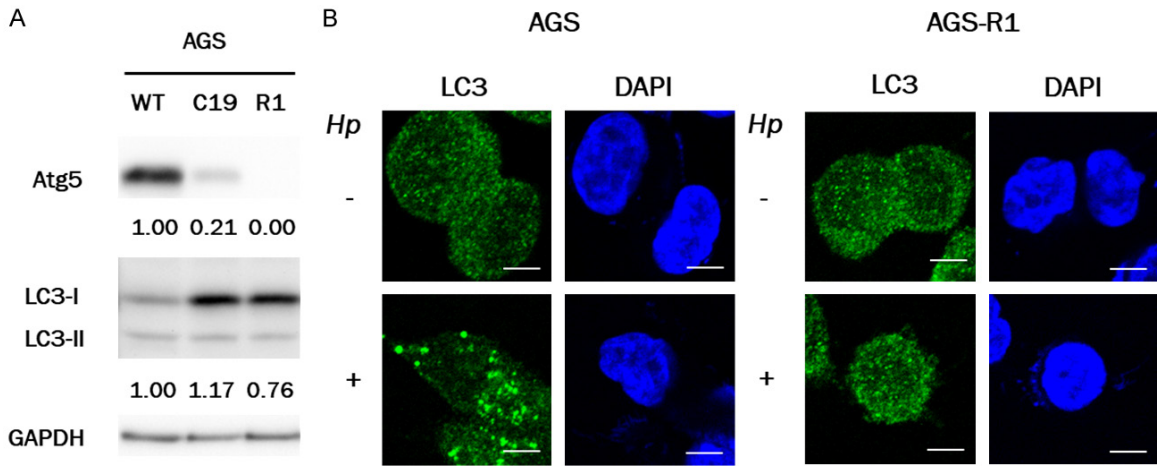

Figure S1. Screening for *Atg5* gene knockout AGS cell lines. Screening for *Atg5* gene knockout AGS clones by the CRISPR-Cas9 system. A. Clone AGS-C19 was the heterologous recombination, and the other clones (AGS-R1, R2, R4) were the homologous recombination. Atg5 protein expression in the cells was detected by Western blotting using anti-Atg5 antibody. GAPDH was used as the internal control. B. AGS and AGS-R1 cells with or without *Hp* 49503 treatment for 24 h were labelled with specific antibodies and visualized under a confocal fluorescent microscope. Scale bar =10 μm.

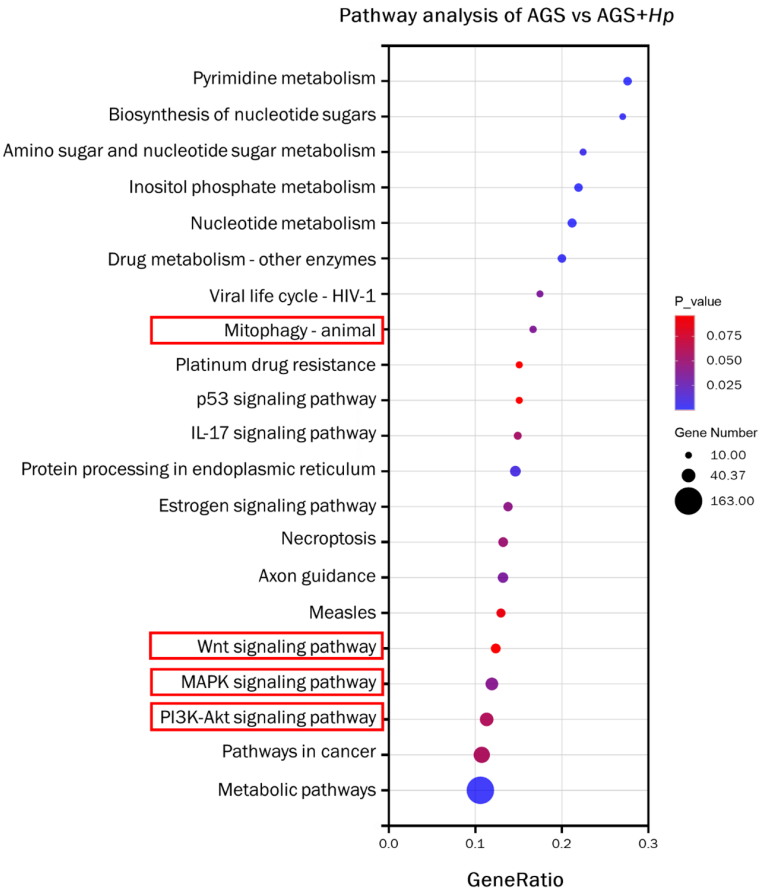

Figure S2. Bubble plot of KEGG pathway enrichment analysis of DEGs. Bubble plots showed differential expression profile-correlated pathways and functions of AGS vs. AGS co-cultured with *H. pylori*. "Gene Number" indicates the number of DEGs enriched in the pathway. "GeneRatio" means the ratio of enriched DEGs to background genes.

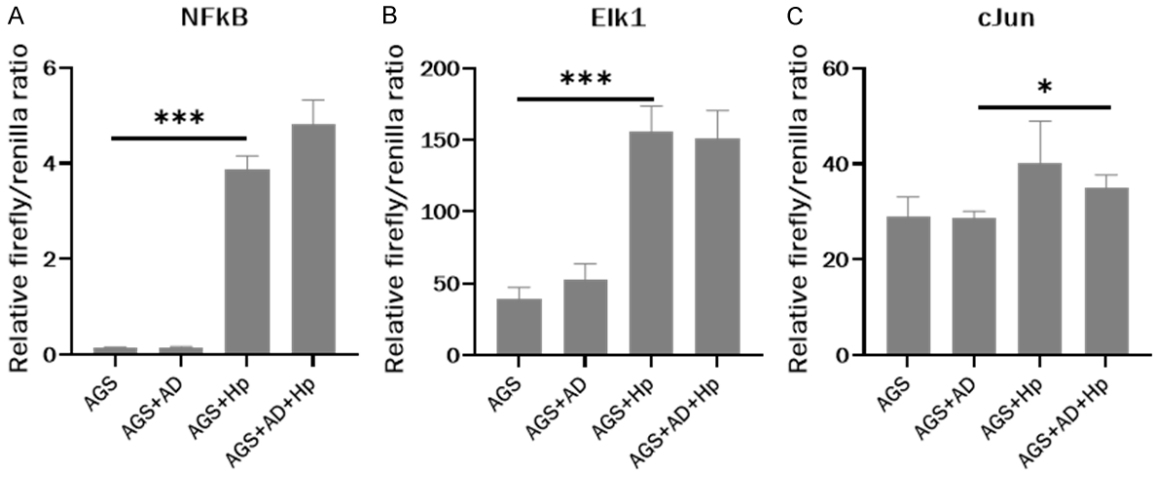

Figure S3. The signaling pathways related to *H. pylori* infection and autophagy induction in GC cells. AGS cells transfected with (A) pNFκB-Luc plasmid. Another reporter plasmid, pFR-Luc, was co-transfected with the (B) pFA2-Elk1 and (C) pFA2-cJun plasmids. Twenty-four hours after transfection, AGS cells were treated with AD (5 μM) for 3 h, followed by removal of AD, and co-culture with *H. pylori* for another 24 h. Luciferase activities were measured from the cell lysates of transfected samples. Values shown are means of three experiments subtracted from the blank control.

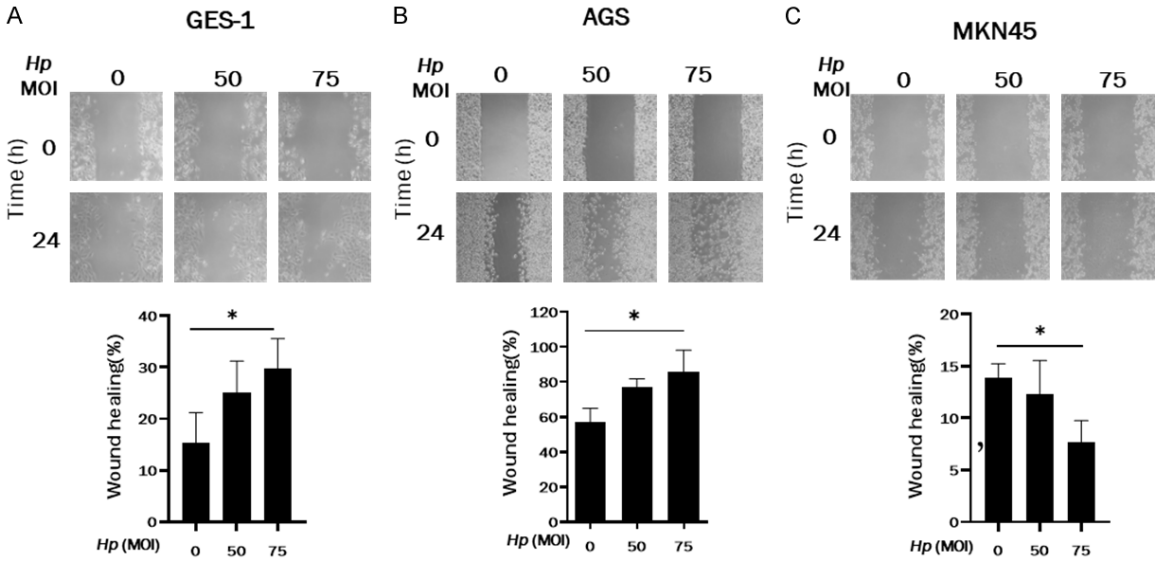

Figure S4. The effect of *Hp* 49503 infection on cell migration by wound healing assay. A wound healing assay was used at 0 h and 24 h after seeding the cells to clarify the effect of *Hp* 49503 infection on cell mobility. The representative images of (A) GES-1, (B) AGS, and (C) MKN45 cell migration under *Hp* 49503 co-culturing conditions were evaluated at 0 h and 24 h by wound healing assay. The white dotted lines represent the migration boundary. Quantification is shown in the diagram. Error bars represent mean ± SD.